Received 6 October 2025; accepted 9 November 2025. Date of publication 12 November 2025; date of current version 21 November 2025.

Digital Object Identifier 10.1109/OJCOMS.2025.3632145

ISAC STAR-RIS Transceivers With Space-Time Coded Pulsed Signals

HEDIEH TAREMIZADEH [1], EMANUELE GROSSI [1,2,3] (Senior Member, IEEE), LUCA VENTURINO [1,2,3] (Senior Member, IEEE), AND MARCO LOPS [3,4] (Fellow, IEEE)

[1]Department of Electrical and Information Engineering, University of Cassino and Southern Lazio, 03043 Cassino, Italy
[2]European University of Technology EUt+, European Union
[3]National Inter-University Consortium for Telecommunications, 43124 Parma, Italy
[4]Department of Electrical Engineering and Information Technology, University of Naples "Federico II," 80138 Naples, Italy

CORRESPONDING AUTHOR: L. VENTURINO (e-mail: l.venturino@unicas.it)

The work of Hedieh Taremizadeh was supported by the Italian Ministry of Education, University, and Research with the Program "Dipartimenti di Eccellenza 2018–2022." The work of Emanuele Grossi was supported by the European Union–Next-GenerationEU–National Recovery and Resilience Plan (NRRP)–Mission 4 Component 2, Investment n. 1.1, Call PRIN 2022 D.D. 104 02-02-2022 (Project 202238BJ2R CIRCE) under Grant CUP H53D23000420006. The work of Luca Venturino was supported by the European Union–Next-GenerationEU–National Recovery and Resilience Plan (NRRP)–Mission 4 Component 2, Investment n. 1.3, Call 341 15-03-2022 (PE00000001, Program "RESTART") under Grant CUP E63C22002040007. The work of Marco Lops was supported by the European Union under the Italian National Recovery and Resilience Plan (PNRR) of NextGenerationEU, Partnership on "Telecommunications of the Future" (PE00000001–Program "RESTART") under Grant–E63C22002040007.

ABSTRACT This work investigates a radar-centric integrated sensing and communication (ISAC) transceiver that incorporates a simultaneous transmitting and reflecting reconfigurable intelligent surface (STAR-RIS) and a radar receiver equipped with a passive electronically scanned array (PESA) and a single digital channel. A periodic pulsed waveform, emitted by a feeder, illuminates the STAR-RIS, which applies space-time modulation to the redirected pulses. The spatial response of the STAR-RIS and the spatial beamformer of the radar receiver are jointly designed to illuminate desired directions on each side of the STAR-RIS, i.e., those monitored by the radar and those corresponding to communication users, while mitigating clutter returns. Time modulation enables both the embedding of communication data and the assignment of unique signatures to echoes from each side of the STAR-RIS. Two encoding schemes are proposed, enabling either simultaneous or sequential illumination of the two sides, while the corresponding radar and communication receivers are designed using a generalized information criterion. Several trade-offs between radar and communication functionalities can be achieved by adjusting the STAR-RIS and PESA array power patterns; in addition, the proposed data encoding schemes allow different data transmission and error rates, while having minimal impact on the radar performance.

INDEX TERMS ISAC, STAR-RIS, space-time coding, generalized information criterion, maximum likelihood decoding, Hadamard matrix.

I. INTRODUCTION

RECONFIGURABLE intelligent surfaces (RISs) are a promising technology for beyond-5G wireless networks [1], [2], [3], [4], [5]. By altering the characteristics of incident signals, they provide a powerful mechanism to control wireless channels, and key benefits include enhanced spectral and energy efficiency, increased coverage, and reduced infrastructure costs. RISs can also superimpose information onto the reflected signals by adjusting the response of their elements across spatial and temporal domains, thereby enabling the implementation of low-cost RIS-based transmitters [6], [7], [8], [9], [10], [11]. RISs are classified into passive and active. Passive RISs are composed of low-power elements without radio-frequency (RF) circuitry and are favored for their energy efficiency, scalability, and ease of deployment[1] [12], [13]. In contrast, active RISs integrate amplifiers and/or RF circuitry to boost the redirected signal power, enable improved control

[1]While we adopt the standard term "passive" here, "nearly passive" is more precise. This is because control circuits are still needed to reconfigure the surfaces, although the power drawn is minimal compared to the power that would be required if RF chains and amplifiers were present.

over beampattern shape, and perform more advanced signal processing at the expense of higher complexity and power consumption [14], [15], [16]. A related concept is Hybrid RIS (HRIS) [17], which combines active and passive elements to mitigate severe path loss and improve robustness against channel estimation errors. HRIS has shown potential in enhancing system performance under challenging propagation conditions, though it introduces additional hardware complexity and power consumption.

Based on their signal redirection capabilities, RISs can also be classified as reflective, transmissive, or simultaneously transmitting and reflecting (STAR-RISs) [18], [19], [20], [21]. STAR-RISs are particularly attractive because they enhance spatial coverage and deployment flexibility. Three operating protocols are introduced in [19] for STAR-RISs: the energy splitting (ES) protocol allows each element to simultaneously reflect and transmit incident signals by allocating a predefined ratio of energy to each direction; the mode switching (MS) protocol assigns each element to operate in either reflection or transmission mode at a given time; finally, the time switching (TS) protocol alternates the entire STAR-RIS between full reflection and full transmission modes over separate time intervals. In this work, we focus on a passive STAR-RIS operating under either the ES or TS protocol. While our system-level design is the primary concern, it is important to acknowledge that STAR-RIS implementations are subject to practical hardware constraints such as phase quantization, nonlinearities, and limited switching speeds. Recent studies [22], [23], [24], [25], [26] have shown that such impairments can significantly impact the performance of metasurface-based architectures in real applications.

In parallel with RIS advancements, integrated sensing and communication (ISAC) has emerged as a key enabler for next-generation wireless systems. ISAC aims to unify communication and sensing functionalities within a single platform, allowing for the joint use of spectral, hardware, and energy resources [27], [28], [29], [30]. Given the complementary strengths of STAR-RIS and ISAC, recent research has explored their integration to optimize system performance [31]. Several aspects of this integration have been explored, including waveform design, beamforming, mobility handling, security, fairness, and hardware realization [32], [33], [34], [35], [36], [37], [38], [39]. The study in [32] presents a beamforming strategy for STAR-RIS-assisted ISAC systems involving multiple radar targets and communication users; the system relies on a dual-functional base station with digital beamforming and signature-sequence modulation to separate radar echoes. In [33], a STAR-RIS assists the base station in target sensing and covert signal transmission under imperfect channel state information (CSI); the joint design of the phase shifts and energy-splitting ratios ensures system reliability under worst-case CSI errors, while physical-layer security techniques mitigate eavesdropping risks. The study in [34] considers a STAR-RIS assisted ISAC system with non-orthogonal multiple access and investigates the problem of serving multiple users under quality-of-service and energy constraints; optimization of phase shifts, energy-splitting ratios, and power allocation improves performance but introduces reliance on iterative convex optimization and accurate CSI, potentially limiting scalability. The study in [35] considers a bi-directional sensing-STARS architecture implementing full-space unlink communication and downlink sensing in a time-switching manner. The concept of *sensing-at-STARS* is instead introduced in [36], where collocated sensors and STAR-RIS elements improve direction-of-arrival estimation under communication constraints; this design assumes partially active elements and treats sensing and communication separately, without waveform-level integration. The work in [38] investigates the use of deep learning for waveform design in ISAC systems assisted by STAR-RISs. Finally, [39] considers an ISAC system assisted by a hybrid STAR-RIS comprising active transmissive and passive reflective elements; in particular, the active elements improve sensing performance by mitigating the two-way attenuation from the base station to the STAR-RIS to the target.

Previous studies on STAR-RIS-enabled ISAC systems have predominantly relied on communication-oriented random waveforms. The proposed approaches often assume full-duplex operation, multichannel digital transceivers, instantaneous CSI, stringent synchronization, and complex algorithms for resource allocation and signal processing. While effective, such designs significantly increase system complexity, energy consumption, and implementation costs. In contrast, this work aims to introduce a simpler approach. Specifically, we leverage a periodic pulse train emitted by a low-cost, single-antenna feeder, which is repurposed by the STAR-RIS to enable sensing and communication. We require that the system operates in half-duplex mode, adopts a monostatic radar configuration, requires only a single digital channel at the radar receiver, eliminates the need for CSI, and employs lightweight signal processing at both the transmitter and receiver. Considering these design choices collectively is novel and can lead to a substantial reduction in complexity and signaling overhead, making the proposed solution suitable for low-cost deployments.

A. CONTRIBUTIONS OF THIS STUDY

Starting from the preliminary ideas presented in [40], [41], this paper proposes the radar-centric ISAC transceiver in Fig. 1, which includes a directional feeder, a passive STAR-RIS, and a radar receiver. The feeder illuminates the STAR-RIS with a periodic pulsed signal, while the STAR-RIS applies space-time modulation to the redirected pulses. The radar receiver is co-located with the STAR-RIS to facilitate synchronization, operates when not illuminated by the feeder to avoid self-interference, and is equipped with a passive electronically scanned array (PESA) using a single digital channel. The main contributions of this work are as follows:

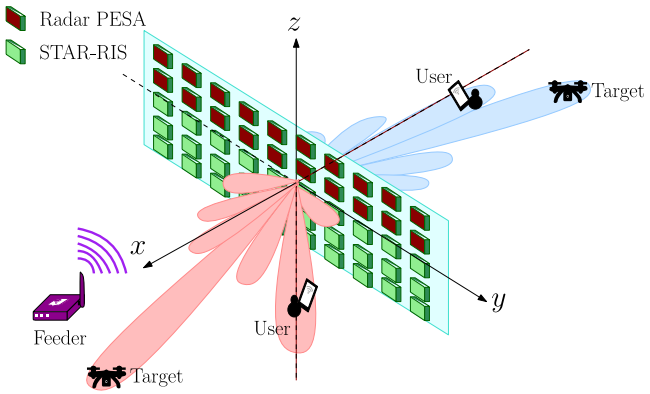

FIGURE 1. Considered system architecture.

- *Joint STAR-RIS and Radar Beamforming Design.* We derive the two-way array power pattern of the monostatic radar, expressed as the product of the STAR-RIS and PESA array power patterns. We then propose a joint design of the STAR-RIS spatial response and the radar analog beamformer to maximize the two-way array power in the directions of prospective radar targets, while suppressing clutter and ensuring minimal radiation toward communication users. This non-convex optimization problem is addressed using the augmented Lagrangian method with partial constraint elimination.
- *Encoding Schemes for STAR-RIS Time-Modulation.* The proposed time-modulation serves a dual purpose: it embeds different data messages and provides unique signatures for radar echoes in each half-space. Building on the ES and TS modes introduced in [19], we propose two encoding schemes that govern the STAR-RIS response over consecutive pulse repetition intervals (PRIs): one enabling simultaneous illumination of both half-spaces, and the other supporting sequential illumination. Both schemes employ orthogonal binary codewords that, for radar, facilitate target separability across half-spaces at the PESA output, and for communication, enable blind data decoding at the user side.
- *Receiver Design.* Under the proposed design framework, the radar detector faces a composite hypothesis testing problem, while the communication receiver needs to blindly estimate the non-zero channel taps for maximum likelihood (ML) decoding. Both tasks involve model order selection, which we address using the generalized information criterion (GIC) [42].
- *Performance Analysis.* We provide a numerical analysis to assess the communication performance, measured in terms of transmission rate and bit error rate (BER), and radar performance, measured in terms of probability of detection (PD) and root mean square error (RMSE) in estimating target radial velocity. Various system tradeoffs can be achieved by reshaping the STAR-RIS and PESA array power patterns; in addition, by changing the time-modulation parameters different tradeoffs between transmission rate and BER can be obtained with minimal impact on radar performance.

B. ORGANIZATION

The remainder of this paper is organized as follows. Section II contains the system description. Section III presents the design of the space-time STAR-RIS response and of the radar and communication receivers. Section IV contains the performance analysis. Section V discusses the conclusions. Finally, some mathematical derivations are deferred to the Appendix.

C. NOTATION

Column vectors/matrices are denoted by lower/uppercase boldface letters. $\mathbb{R}$ and $\mathbb{C}$ are the set of real and complex numbers, respectively. The symbols i, $(\cdot)^*$, $(\cdot)^{\mathsf{T}}$, $(\cdot)^{\mathsf{H}}$, $\mathrm{Tr}(\cdot)$, $\Re(\cdot)$, $*$ and $\otimes$ denote the imaginary unit, conjugate, transpose, conjugate-transpose, trace, real part, convolution, and Kronecker product, respectively. $\mathbb{E}[\cdot]$ denotes the statistical expectation. $[\boldsymbol{x}]_{a:b}$ is the subvector of $\boldsymbol{x}$ containing entries from position a to b. $[\boldsymbol{A}]_{i,j}$ is the entry in the i-th row and j-th column of $\boldsymbol{A}$. $[\boldsymbol{A}_1 \ \cdots \ \boldsymbol{A}_n]$ and $[\boldsymbol{A}_1; \ \cdots; \boldsymbol{A}_n]$ are the horizontal and vertical concatenations of $\boldsymbol{A}_1, \ldots, \boldsymbol{A}_n$, respectively. $\boldsymbol{I}_M$ is the $M \times M$ identity matrix. $\boldsymbol{0}_M$ is the M-dimensional vector with all zero entries. $\mathrm{diag}\{\boldsymbol{x}\}$ is a diagonal matrix with $\boldsymbol{x}$ on the main diagonal. $\mathbb{1}_{\mathcal{A}}$ is the indicator function of the condition $\mathcal{A}$, i.e., $\mathbb{1}_{\mathcal{A}} = 1$, if $\mathcal{A}$ is verified, and $\mathbb{1}_{\mathcal{A}} = 0$, otherwise. $\mathrm{card}(\mathcal{A})$ denotes the cardinality of the set $\mathcal{A}$. x^+ is equal to x, if $x \geq 0$, and to 0, otherwise. Finally, $\|\cdot\|_F$, $\|\cdot\|_p$, and $\|\cdot\|_\infty$ denote the Frobenius norm, the p-norm, and the ∞-norm, respectively.

II. SYSTEM DESCRIPTION

We consider the system in Fig. 1 that operates at the carrier frequency f_o. The feeder is equipped with a directional antenna illuminating the STAR-RIS and emits the baseband pulse train

$$\sum_{p=-\infty}^{+\infty} \sqrt{\mathcal{E}}\psi(t - pT + \delta), \tag{1}$$

where: $\psi(t)$ is a unit-energy pulse with bandwidth B that is zero if $t \notin [0, \Delta)$, with $\Delta \simeq 1/B$; $\mathcal{E} = \mathcal{P}\Delta$ is the pulse energy; $\mathcal{P}$ is the pulse power; T is the pulse repetition interval (PRI), with $T \gg \Delta$; δ is time of flight between the feeder and STAR-RIS. The feeder may be a dedicated device or a collaborative access point. The STAR-RIS has N_{ris} atoms and divides the space into the transmissive and reflective half-spaces. The STAR-RIS aims to illuminate the angular region monitored by the radar receiver and to communicate with a single antenna user in each half-space. Users do not experience multiple access interference due to the spatial separation induced by the STAR-RIS. The radar receiver is equipped with a PESA containing N_{rad} antennas that simultaneously collects the echoes from both half-spaces. The STAR-RIS and PESA elements are organized into two

collocated uniform rectangular arrays, which lay on the (y, z)-plane of a Cartesian reference system centered at their center of gravity, as shown in Fig. 1, with the positive x-axis pointing towards the reflective half-space; hence, the azimuth angle belongs to $(\pi/2, 3\pi/2)$ and $(-\pi/2, \pi/2)$ in the transmissive and reflective half-spaces, respectively. After analog beamforming, the radar elaborates the received signal via a single digital channel over a coherent processing interval (CPI) spanning P PRIs. Without loss of generality, the CPI $[0, PT)$ is considered for illustration.

To proceed, we make the following assumptions.

- The sizes of the STAR-RIS and of the radar receiving array are much smaller than c/B, where c is the speed of light (narrowband assumption [43]); also, any mutual coupling among their atoms/antennas is neglected.
- The STAR-RIS and radar receiver are synchronized and aware of the feeder's timing. The synchronization between STAR-RIS and radar receiver can be easily achieved since the two systems are collocated and (possibly) share the same clock. To avoid direct interference, the radar receiver operates when the feeder is not transmitting; consequently, the STAR-RIS atoms may also be used for reception if equipped with necessary circuitry[44].
- The channel $\boldsymbol{g} \in \mathbb{C}^{N_{\rm ris}}$ between the feeder and STAR-RIS is known to the STAR-RIS-based transceiver, and it remains constant over the CPI. This can easily be achieved, as the feeder and the STAR-RIS belong to the same network and are coordinated by a common control unit.
- Prospective targets are point-like and located in the far-field of the STAR-RIS and the radar PESA.
- The users do not have instantaneous CSI; specifically, angles of arrival, amplitudes, and delays of the multipath channel are unknown. They only have statistical information about the channel's delay spread and are aware of the encoder timing.
- The STAR-RIS does not have instantaneous CSI; specifically, angles of departure, amplitudes, and delays of the multipath channel are unknown. It may only have some prior information about the users' locations, encapsulated in the uncertainty set where the angles of departure belong.

For future reference, we denote by $\boldsymbol{\phi} = [\phi^{\rm az}; \phi^{\rm el}]$ the angular direction with azimuth angle $\phi^{\rm az}$ and elevation angle $\phi^{\rm el}$; accordingly, the sets $\mathcal{F}_{\rm tr} = (\frac{\pi}{2}, \frac{3\pi}{2}) \times (-\frac{\pi}{2}, \frac{\pi}{2})$ and $\mathcal{F}_{\rm re} = (-\frac{\pi}{2}, \frac{\pi}{2}) \times (-\frac{\pi}{2}, \frac{\pi}{2})$ contain all angular directions in the transmissive and reflective half-spaces, respectively, while $\mathcal{F} = \mathcal{F}_{\rm tr} \cup \mathcal{F}_{\rm re}$ specify the entire field of view. Also, we denote by $G_{\rm ris}(\boldsymbol{\phi})$ and $G_{\rm rad}(\boldsymbol{\phi})$ the element gains of the STAR-RIS and radar receiving array towards $\boldsymbol{\phi}$, respectively. Finally, $\boldsymbol{u}_{\rm ris}(\boldsymbol{\phi}) \in \mathbb{C}^{N_{\rm ris}}$ and $\boldsymbol{u}_{\rm rad}(\boldsymbol{\phi}) \in \mathbb{C}^{N_{\rm rad}}$ are the steering vectors of the STAR-RIS and radar receiving array towards $\boldsymbol{\phi}$, respectively; in particular, we have [43]

$$\boldsymbol{u}_{\rm rad}(\boldsymbol{\phi}) = \Big[1; \mathrm{e}^{\mathrm{i}\frac{2\pi d_{\rm rad}}{\lambda}\sin\phi^{\rm el}}; \cdots; \mathrm{e}^{\mathrm{i}(N_{{\rm rad},z}-1)\frac{2\pi d_{\rm rad}}{\lambda}\sin\phi^{\rm el}}\Big] \otimes \Big[1; \mathrm{e}^{\mathrm{i}\frac{2\pi d_{\rm rad}}{\lambda}\cos\phi^{\rm el}\sin\phi^{\rm az}}; \cdots; \mathrm{e}^{\mathrm{i}(N_{{\rm rad},y}-1)\frac{2\pi d_{\rm rad}}{\lambda}\cos\phi^{\rm el}\sin\phi^{\rm az}}\Big], \quad (2)$$

where λ is the carrier wavelength, $N_{{\rm rad},y}$ and $N_{{\rm rad},z}$ are the number of elements along the y and z axes, respectively, $N_{\rm rad} = N_{{\rm rad},y}N_{{\rm rad},z}$, and $d_{\rm rad}$ is the element spacing; $\boldsymbol{u}_{\rm ris}(\boldsymbol{\phi})$ is similarly defined. Finally, to aid in following the system's description and the mathematical derivations, a list of key variables and symbols defined and used throughout this section is provided in Table 1.

A. SPACE-TIME STAR-RIS RESPONSE

In the p-th PRI, the STAR-RIS response in the transmissive and reflective half-spaces is

$$c_{\rm tr}(p)\boldsymbol{s}_{\rm tr} \in \mathbb{C}^{N_{\rm ris}}, \quad (3a)$$

$$c_{\rm re}(p)\boldsymbol{s}_{\rm re} \in \mathbb{C}^{N_{\rm ris}}, \quad (3b)$$

respectively, where $\boldsymbol{s}_{\rm tr}$ and $\boldsymbol{s}_{\rm re}$ are $N_{\rm ris}$–dimensional spatial beamformers with unit modulus entries, while $c_{\rm tr}(p)$ and $c_{\rm re}(p)$ are complex scalars with $|c_{\rm tr}(p)|^2 + |c_{\rm re}(p)|^2 = 1$, for $p = 0, \ldots, P-1$. Accordingly, the signal redirected by the STAR-RIS towards $\boldsymbol{\phi} \in \mathcal{F}$ is

$$\varrho_{\rm RIS}(t, \boldsymbol{\phi}) = \varrho_{\rm tr}(t, \boldsymbol{\phi}) + \varrho_{\rm re}(t, \boldsymbol{\phi}), \quad (4)$$

for $t \in [0, PT)$, where

$$\varrho_{\rm tr}(t, \boldsymbol{\phi}) = \mathbb{1}_{\{\boldsymbol{\phi}\in\mathcal{F}_{\rm tr}\}}\sqrt{\mathcal{E}G_{\rm ris}(\boldsymbol{\phi})}\big(\boldsymbol{u}_{\rm ris}^{\mathsf{T}}(\boldsymbol{\phi})\mathrm{diag}\{\boldsymbol{s}_{\rm tr}\}\boldsymbol{g}\big) \times \sum_{p=0}^{P-1} c_{\rm tr}(p)\psi(t-pT), \quad (5a)$$

$$\varrho_{\rm re}(t, \boldsymbol{\phi}) = \mathbb{1}_{\{\boldsymbol{\phi}\in\mathcal{F}_{\rm re}\}}\sqrt{\mathcal{E}G_{\rm ris}(\boldsymbol{\phi})}\big(\boldsymbol{u}_{\rm ris}^{\mathsf{T}}(\boldsymbol{\phi})\mathrm{diag}\{\boldsymbol{s}_{\rm re}\}\boldsymbol{g}\big) \times \sum_{p=0}^{P-1} c_{\rm re}(p)\psi(t-pT). \quad (5b)$$

The space-time STAR-RIS response is under the designer's control; in particular, by inspecting (4), the following remarks are in order.

Remark 1: The terms $G_{\rm ris}(\boldsymbol{\phi})|\boldsymbol{u}_{\rm ris}^{\mathsf{T}}(\boldsymbol{\phi})\mathrm{diag}\{\boldsymbol{s}_{\rm tr}\}\boldsymbol{g}|^2$ and $G_{\rm ris}(\boldsymbol{\phi})|\boldsymbol{u}_{\rm ris}^{\mathsf{T}}(\boldsymbol{\phi})\mathrm{diag}\{\boldsymbol{s}_{\rm re}\}\boldsymbol{g}|^2$ specify the intensity of the electromagnetic signals redirected by the STAR-RIS towards $\boldsymbol{\phi} \in \mathcal{F}_{\rm tr}$ and $\boldsymbol{\phi} \in \mathcal{F}_{\rm re}$, respectively. In particular, we define the STAR-RIS array power pattern as

$$\mathrm{A}_{\rm ris}(\boldsymbol{\phi}; \boldsymbol{s}_{\rm tr}, \boldsymbol{s}_{\rm re}) = \mathrm{A}_{\rm tr}(\boldsymbol{\phi}; \boldsymbol{s}_{\rm tr}) + \mathrm{A}_{\rm re}(\boldsymbol{\phi}; \boldsymbol{s}_{\rm re}), \quad (6)$$

for $\boldsymbol{\phi} \in \mathcal{F}$, where

$$\mathrm{A}_{\rm tr}(\boldsymbol{\phi}; \boldsymbol{s}_{\rm tr}) = \frac{\big|\boldsymbol{u}_{\rm ris}^{\mathsf{T}}(\boldsymbol{\phi})\mathrm{diag}\{\boldsymbol{s}_{\rm tr}\}\boldsymbol{g}\big|^2}{\|\boldsymbol{g}\|_1^2}\mathbb{1}_{\{\boldsymbol{\phi}\in\mathcal{F}_{\rm tr}\}} \quad (7a)$$

$$\mathrm{A}_{\rm re}(\boldsymbol{\phi}; \boldsymbol{s}_{\rm re}) = \frac{\big|\boldsymbol{u}_{\rm ris}^{\mathsf{T}}(\boldsymbol{\phi})\mathrm{diag}\{\boldsymbol{s}_{\rm re}\}\boldsymbol{g}\big|^2}{\|\boldsymbol{g}\|_1^2}\mathbb{1}_{\{\boldsymbol{\phi}\in\mathcal{F}_{\rm re}\}} \quad (7b)$$

are the STAR-RIS array power patterns in the transmissive and reflective half-spaces, respectively. In (6), we have made explicit the dependence upon $\boldsymbol{s}_{\rm tr}$ and $\boldsymbol{s}_{\rm re}$; these beamformers will be designed in Section III-A to redirect the incident

TABLE 1. List of key variables and symbols.

λ = Carrier wavelength
T = Pulse repetition interval
$\mathcal{E}$ = Pulse energy
$N_{\rm ris}$ = Number of elements of the STAR-RIS
$N_{\rm rad}$ = Number of elements of the radar PESA
$G_{\rm ris}(\phi)$ = Element gain of the STAR-RIS
$G_{\rm rad}(\phi)$ = Element gain of the radar PESA
$\boldsymbol{g}$ = Radar transmitter to STAR-RIS channel
P = Number of pulses in the CPI at the radar receiver
$\mathcal{F}_{\rm tr}$ = Angular directions in the tr. side
$\mathcal{F}_{\rm re}$ = Angular directions in the re. side
$\mathcal{F} = \mathcal{F}_{\rm tr} \cup \mathcal{F}_{\rm re}$ = STAR-RIS field of view
$\boldsymbol{u}_{\rm ris}(\phi)$ = Steering vector of the STAR-RIS
$\boldsymbol{u}_{\rm rad}(\phi)$ = Steering vector of the radar PESA
$\boldsymbol{s}_{\rm rad}$ = Radar receiver analog beamformer
$c_{\rm tr}(p)\boldsymbol{s}_{\rm tr}$ = STAR-RIS space-time response (tr. side)
$c_{\rm re}(p)\boldsymbol{s}_{\rm re}$ = STAR-RIS space-time response (re. side)
$\boldsymbol{c}_{\rm tr} = [c_{\rm tr}(0); \cdots ; c_{\rm tr}(P-1)]$ = Code sequence (tr. side)
$\boldsymbol{c}_{\rm re} = [c_{\rm re}(0); \cdots ; c_{\rm re}(P-1)]$ = Code sequence (re. side)
$\mathrm{A}_{\rm tr}(\phi; \boldsymbol{s}_{\rm tr}) = \lvert\boldsymbol{u}_{\rm ris}^{\mathsf{T}}(\phi)\mathrm{diag}\{\boldsymbol{s}_{\rm tr}\}\boldsymbol{g}\rvert^2 \lVert\boldsymbol{g}\rVert_1^{-2} \mathbb{1}_{\{\phi\in\mathcal{F}_{\rm tr}\}}$ = STAR-RIS array power pattern (tr. side)
$\mathrm{A}_{\rm re}(\phi; \boldsymbol{s}_{\rm re}) = \lvert\boldsymbol{u}_{\rm ris}^{\mathsf{T}}(\phi)\mathrm{diag}\{\boldsymbol{s}_{\rm re}\}\boldsymbol{g}\rvert^2 \lVert\boldsymbol{g}\rVert_1^{-2} \mathbb{1}_{\{\phi\in\mathcal{F}_{\rm re}\}}$ = STAR-RIS array power pattern (re. side)
$\mathrm{A}_{\rm ris}(\phi; \boldsymbol{s}_{\rm tr}, \boldsymbol{s}_{\rm re}) = \mathrm{A}_{\rm tr}(\phi; \boldsymbol{s}_{\rm tr}) + \mathrm{A}_{\rm re}(\phi; \boldsymbol{s}_{\rm re})$ = Array power pattern of the STAR-RIS
$\mathrm{A}_{\rm rad}(\phi; \boldsymbol{s}_{\rm rad}) = \lvert\boldsymbol{s}_{\rm rad}^{\mathsf{H}}\boldsymbol{u}_{\rm rad}(\phi)\rvert^2 N_{\rm rad}^{-2}$ = Array power pattern of the radar PESA
$\mathrm{A}(\phi; \boldsymbol{s}_{\rm tr}, \boldsymbol{s}_{\rm re}, \boldsymbol{s}_{\rm rad}) = \mathrm{A}_{\rm rad}(\phi; \boldsymbol{s}_{\rm rad})\mathrm{A}_{\rm ris}(\phi; \boldsymbol{s}_{\rm tr}, \boldsymbol{s}_{\rm re})$ = Two-way array power pattern
$\gamma_{\rm tr}(\phi; \boldsymbol{s}_{\rm tr}, \boldsymbol{s}_{\rm rad}) = \sqrt{\frac{\mathcal{E}G_{\rm rad}(\phi)G_{\rm ris}(\phi)\lambda^2}{4\pi N_{\rm rad}}} (\boldsymbol{s}_{\rm rad}^{\mathsf{H}}\boldsymbol{u}_{\rm rad}(\phi)) \times (\boldsymbol{u}_{\rm ris}^{\mathsf{T}}(\phi)\mathrm{diag}\{\boldsymbol{g}\}\boldsymbol{s}_{\rm tr})\mathbb{1}_{\{\phi\in\mathcal{F}_{\rm tr}\}}$ = Two-way field response (tr. side)
$\gamma_{\rm re}(\phi; \boldsymbol{s}_{\rm re}, \boldsymbol{s}_{\rm rad}) = \sqrt{\frac{\mathcal{E}G_{\rm rad}(\phi)G_{\rm ris}(\phi)\lambda^2}{4\pi N_{\rm rad}}} (\boldsymbol{s}_{\rm rad}^{\mathsf{H}}\boldsymbol{u}_{\rm rad}(\phi)) \times (\boldsymbol{u}_{\rm ris}^{\mathsf{T}}(\phi)\mathrm{diag}\{\boldsymbol{g}\}\boldsymbol{s}_{\rm re})\mathbb{1}_{\{\phi\in\mathcal{F}_{\rm re}\}}$ = Two-way field response (re. side)
$\gamma(\phi; \boldsymbol{s}_{\rm tr}, \boldsymbol{s}_{\rm re}, \boldsymbol{s}_{\rm rad}) = \gamma_{\rm tr}(\phi; \boldsymbol{s}_{\rm tr}, \boldsymbol{s}_{\rm rad}) + \gamma_{\rm re}(\phi; \boldsymbol{s}_{\rm re}, \boldsymbol{s}_{\rm rad})$ = Two way field response
$\boldsymbol{h}(\boldsymbol{c}, \nu) = [c(0); c(1)\mathrm{e}^{\mathrm{i}2\pi T\nu}; \cdots ; c(P-1)\mathrm{e}^{\mathrm{i}2\pi\nu T(P-1)}]$ = Doppler-shifted code sequence

signal towards some desired directions. Also, the adopted normalization ensures that $\mathrm{A}_{\rm ris}(\boldsymbol{\phi}; \boldsymbol{s}_{\rm tr}, \boldsymbol{s}_{\rm re}) \leq 1\ \forall \boldsymbol{\phi} \in \mathcal{F}$.

Remark 2: The P-dimensional code sequences

$$\boldsymbol{c}_{\rm tr} = [c_{\rm tr}(0); \cdots ; c_{\rm tr}(P-1)] \tag{8a}$$

$$\boldsymbol{c}_{\rm re} = [c_{\rm re}(0); \cdots ; c_{\rm re}(P-1)] \tag{8b}$$

superimpose a time modulation on the pulses redirected in the transmissive and reflective half-spaces, respectively; these code sequences will be designed in Section III-B to enable the sensing and communication functions.

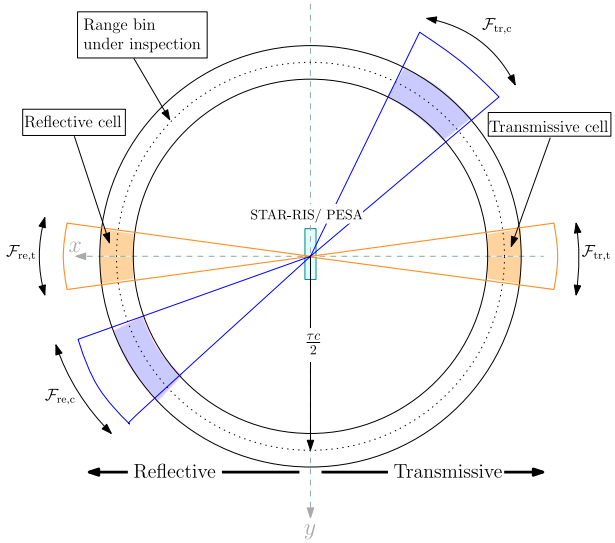

FIGURE 2. Illustration of the transmissive and reflective cells inspected by the radar receiver and of the clutter regions.

B. RADAR RECEIVED SIGNAL

Denote by $\boldsymbol{s}_{\rm rad} \in \mathbb{C}^{N_{\rm rad}}$ the analog beamformer with unit modulus entries employed by the radar receiver. This beamformer is under the designer's control and determines the PESA array power pattern, defined as

$$\mathrm{A}_{\rm rad}(\boldsymbol{\phi}; \boldsymbol{s}_{\rm rad}) = \frac{\left|\boldsymbol{s}_{\rm rad}^{\mathsf{H}}\boldsymbol{u}_{\rm rad}(\boldsymbol{\phi})\right|^2}{N_{\rm rad}^2}, \tag{9}$$

for $\boldsymbol{\phi} \in \mathcal{F}$ (more on this in Section III). The adopted normalization ensures that $\mathrm{A}_{\rm rad}(\boldsymbol{\phi}; \boldsymbol{s}_{\rm rad}) \leq 1\ \forall \boldsymbol{\phi} \in \mathcal{F}$.

From (2), it is seen that $\boldsymbol{u}_{\rm rad}([\phi^{\rm az}; \phi^{\rm el}]) = \boldsymbol{u}_{\rm rad}([\pi - \phi^{\rm az}; \phi^{\rm el}])$ for any $\phi^{\rm az} \in (-\pi/2, \pi/2)$, which in turn implies $\mathrm{A}_{\rm rad}([\phi^{\rm az}; \phi^{\rm el}]; \boldsymbol{s}_{\rm rad}) = \mathrm{A}_{\rm rad}([\pi - \phi^{\rm az}; \phi^{\rm el}]; \boldsymbol{s}_{\rm rad})$. To reflect such symmetry, the angular regions monitored by the radar receiver in the transmissive and reflective half-spaces, say $\mathcal{F}_{\rm tr,t} \subset \mathcal{F}_{\rm tr}$ and $\mathcal{F}_{\rm re,t} \subset \mathcal{F}_{\rm re}$, respectively, are chosen mirror symmetric with respect to the plane containing both the STAR-RIS and the radar receiving array, as shown in Fig. 2; more specifically, we assume that

$$\mathcal{F}_{\rm tr,t} = \left[\varphi_{\rm tr,t}^{\rm az} - \Delta_{\rm t}^{\rm az}, \varphi_{\rm tr,t}^{\rm az} + \Delta_{\rm t}^{\rm az}\right] \times \left[\varphi_{\rm tr,t}^{\rm el} - \Delta_{\rm t}^{\rm el}, \varphi_{\rm tr,t}^{\rm el} + \Delta_{\rm t}^{\rm el}\right], \tag{10a}$$

$$\mathcal{F}_{\rm re,t} = \left[\varphi_{\rm re,t}^{\rm az} - \Delta_{\rm t}^{\rm az}, \varphi_{\rm re,t}^{\rm az} + \Delta_{\rm t}^{\rm az}\right] \times \left[\varphi_{\rm re,t}^{\rm el} - \Delta_{\rm t}^{\rm el}, \varphi_{\rm re,t}^{\rm el} + \Delta_{\rm t}^{\rm el}\right], \tag{10b}$$

respectively, with $\varphi_{\rm re,t}^{\rm az} = \pi - \varphi_{\rm tr,t}^{\rm az}$ and $\varphi_{\rm re,t}^{\rm el} = \varphi_{\rm tr,t}^{\rm el}$; here, $\boldsymbol{\varphi}_{\rm tr,t} = [\varphi_{\rm tr,t}^{\rm az}; \varphi_{\rm tr,t}^{\rm el}]$ and $\boldsymbol{\varphi}_{\rm re,t} = [\varphi_{\rm re,t}^{\rm az}; \varphi_{\rm re,t}^{\rm el}]$ are the central directions, while $\Delta_{\rm t}^{\rm az}$ and $\Delta_{\rm t}^{\rm el}$ specify the size of these regions. For future reference, we also define $\mathcal{F}_{\rm t} = \mathcal{F}_{\rm tr,t} \cup \mathcal{F}_{\rm re,t}$.

Next, denote by $\boldsymbol{b}_{\rm rad}(t) \in \mathbb{C}^{N_{\rm rad}}$ the baseband continuous-time signal collected by the antennas of the radar receiver in the considered CPI and by τ the delay of the inspected

range bin. After analog beamforming, pulse compression, and range gating, the following samples are obtained

$$y_{\mathrm{rad}}(p) = \frac{1}{\sqrt{N_{\mathrm{rad}}}} \int_{\mathbb{R}} \boldsymbol{s}_{\mathrm{rad}}^{\mathsf{H}} \boldsymbol{b}_{\mathrm{rad}}(t) \psi^*\big(t - pT - \tau\big) dt, \quad (11)$$

for $p = 0, \ldots, P-1$. The pairs $(\boldsymbol{\varphi}_{\mathrm{tr,t}}, \tau)$ and $(\boldsymbol{\varphi}_{\mathrm{re,t}}, \tau)$ specify the resolution cells under inspection, as depicted in Fig. 2: we refer to them as the transmissive and reflective cells, respectively. For any $\boldsymbol{\phi} \in \mathcal{F}$, define the two-way field response in the transmissive and reflective side as

$$\gamma_{\mathrm{tr}}(\boldsymbol{\phi}; \boldsymbol{s}_{\mathrm{tr}}, \boldsymbol{s}_{\mathrm{rad}}) = \sqrt{\frac{\mathcal{E} G_{\mathrm{rad}}(\boldsymbol{\phi}) G_{\mathrm{ris}}(\boldsymbol{\phi}) \lambda^2}{4\pi N_{\mathrm{rad}}}} \big(\boldsymbol{s}_{\mathrm{rad}}^{\mathsf{H}} \boldsymbol{u}_{\mathrm{rad}}(\boldsymbol{\phi})\big) \times \big(\boldsymbol{u}_{\mathrm{ris}}^{\mathsf{T}}(\boldsymbol{\phi}) \mathrm{diag}\{\boldsymbol{g}\} \boldsymbol{s}_{\mathrm{tr}}\big) \mathbb{1}_{\{\boldsymbol{\phi} \in \mathcal{F}_{\mathrm{tr}}\}}, \quad (12a)$$

$$\gamma_{\mathrm{re}}(\boldsymbol{\phi}; \boldsymbol{s}_{\mathrm{re}}, \boldsymbol{s}_{\mathrm{rad}}) = \sqrt{\frac{\mathcal{E} G_{\mathrm{rad}}(\boldsymbol{\phi}) G_{\mathrm{ris}}(\boldsymbol{\phi}) \lambda^2}{4\pi N_{\mathrm{rad}}}} \big(\boldsymbol{s}_{\mathrm{rad}}^{\mathsf{H}} \boldsymbol{u}_{\mathrm{rad}}(\boldsymbol{\phi})\big) \times \big(\boldsymbol{u}_{\mathrm{ris}}^{\mathsf{T}}(\boldsymbol{\phi}) \mathrm{diag}\{\boldsymbol{g}\} \boldsymbol{s}_{\mathrm{re}}\big) \mathbb{1}_{\{\boldsymbol{\phi} \in \mathcal{F}_{\mathrm{re}}\}}, \quad (12b)$$

respectively, which account for overall propagation effects, except for the target response and the temporal modulation induced by the STAR-RIS. Upon assuming that at most one target is present in each resolution cell, $y_{\mathrm{rad}}(p)$ can be expanded as

$$y_{\mathrm{rad}}(p) = \alpha_{\mathrm{tr,t}} \gamma_{\mathrm{tr}}\big(\boldsymbol{\phi}_{\mathrm{tr,t}}; \boldsymbol{s}_{\mathrm{tr}}, \boldsymbol{s}_{\mathrm{rad}}\big) c_{\mathrm{tr}}(p) \mathrm{e}^{\mathrm{i}2\pi \nu_{\mathrm{tr,t}} T(p-1)} + \alpha_{\mathrm{re,t}} \gamma_{\mathrm{re}}\big(\boldsymbol{\phi}_{\mathrm{re,t}}; \boldsymbol{s}_{\mathrm{re}}, \boldsymbol{s}_{\mathrm{rad}}\big) c_{\mathrm{re}}(p) \mathrm{e}^{\mathrm{i}2\pi \nu_{\mathrm{re,t}} T(p-1)} + z_{\mathrm{rad}}(p), \quad (13)$$

where: $\alpha_{\mathrm{tr,t}} \in \mathbb{C}$, $\nu_{\mathrm{tr,t}} \in \mathbb{R}$, and $\boldsymbol{\phi}_{\mathrm{tr,t}} \in \mathcal{F}_{\mathrm{tr,t}}$ are the unknown amplitude, Doppler shift, and angular direction of a prospective target in the transmissive cell, respectively; $\alpha_{\mathrm{re,t}} \in \mathbb{C}$, $\nu_{\mathrm{re,t}} \in \mathbb{R}$, and $\boldsymbol{\phi}_{\mathrm{re,t}} \in \mathcal{F}_{\mathrm{re,t}}$ are the unknown amplitude, Doppler shift, and angular direction of a prospective target in the reflective cell, respectively; $z_{\mathrm{rad}}(p)$ is the additive disturbance, including both clutter and noise. Here, $\alpha_{\mathrm{tr,t}}$ and $\alpha_{\mathrm{re,t}}$ account for the two-way path-loss from the STAR-RIS to the target and the target radar cross-section (RCS), with $\alpha_{\mathrm{tr,t}} = 0$ and $\alpha_{\mathrm{re,t}} = 0$ if no target is present in the transmissive and reflective cells, respectively.

The observations in (13) are collected into the vector $\boldsymbol{y}_{\mathrm{rad}} = [y_{\mathrm{rad}}(0); \cdots; y_{\mathrm{rad}}(P-1)] \in \mathbb{C}^P$. For any code sequence $\boldsymbol{c} = [c(0); \cdots; c(P-1)] \in \mathbb{C}^P$ and Doppler shift $\nu \in \mathbb{R}$, denote by

$$\boldsymbol{h}(\boldsymbol{c}, \nu) = \Big[c(0); c(1)\mathrm{e}^{\mathrm{i}2\pi T \nu}; \cdots; c(P-1)\mathrm{e}^{\mathrm{i}2\pi \nu T(P-1)}\Big] \quad (14)$$

the corresponding Doppler-shifted code sequence. Then, we have

$$\boldsymbol{y}_{\mathrm{rad}} = \alpha_{\mathrm{tr,t}} \gamma_{\mathrm{tr}}\big(\boldsymbol{\phi}_{\mathrm{tr,t}}; \boldsymbol{s}_{\mathrm{tr}}, \boldsymbol{s}_{\mathrm{rad}}\big) \boldsymbol{h}\big(\boldsymbol{c}_{\mathrm{tr}}, \nu_{\mathrm{tr,t}}\big) \quad (15)$$

$$+ \alpha_{\mathrm{re,t}} \gamma_{\mathrm{re}}\big(\boldsymbol{\phi}_{\mathrm{re,t}}; \boldsymbol{s}_{\mathrm{re}}, \boldsymbol{s}_{\mathrm{rad}}\big) \boldsymbol{h}\big(\boldsymbol{c}_{\mathrm{re}}, \nu_{\mathrm{re,t}}\big) + \boldsymbol{z}_{\mathrm{rad}}, \quad (16)$$

where $\boldsymbol{z}_{\mathrm{rad}} = [z_{\mathrm{rad}}(0); \cdots; z_{\mathrm{rad}}(P-1)] \in \mathbb{C}^P$.

1) TWO-WAY ARRAY POWER PATTERN

For $\boldsymbol{\phi} \in \mathcal{F}$, the quantity

$$\gamma(\boldsymbol{\phi}; \boldsymbol{s}_{\mathrm{tr}}, \boldsymbol{s}_{\mathrm{re}}, \boldsymbol{s}_{\mathrm{rad}}) = \gamma_{\mathrm{tr}}(\boldsymbol{\phi}; \boldsymbol{s}_{\mathrm{tr}}, \boldsymbol{s}_{\mathrm{rad}}) + \gamma_{\mathrm{re}}(\boldsymbol{\phi}; \boldsymbol{s}_{\mathrm{re}}, \boldsymbol{s}_{\mathrm{rad}}) \quad (17)$$

depends on the two-way spatial response of the radar; in particular, we have

$$|\gamma(\boldsymbol{\phi}; \boldsymbol{s}_{\mathrm{tr}}, \boldsymbol{s}_{\mathrm{re}}, \boldsymbol{s}_{\mathrm{rad}})|^2 = \frac{\mathcal{E} G_{\mathrm{rad}}(\boldsymbol{\phi}) G_{\mathrm{ris}}(\boldsymbol{\phi}) \lambda^2}{4\pi} N_{\mathrm{rad}} \times \|\boldsymbol{g}\|_1^2 \mathrm{A}(\boldsymbol{\phi}; \boldsymbol{s}_{\mathrm{tr}}, \boldsymbol{s}_{\mathrm{re}}, \boldsymbol{s}_{\mathrm{rad}}), \quad (18)$$

where

$$\mathrm{A}(\boldsymbol{\phi}; \boldsymbol{s}_{\mathrm{tr}}, \boldsymbol{s}_{\mathrm{re}}, \boldsymbol{s}_{\mathrm{rad}}) = \mathrm{A}_{\mathrm{rad}}(\boldsymbol{\phi}; \boldsymbol{s}_{\mathrm{rad}}) \mathrm{A}_{\mathrm{ris}}(\boldsymbol{\phi}; \boldsymbol{s}_{\mathrm{tr}}, \boldsymbol{s}_{\mathrm{re}}) \quad (19)$$

is the two-way array power pattern towards $\boldsymbol{\phi} \in \mathcal{F}$. Notice that $\mathrm{A}(\boldsymbol{\phi}; \boldsymbol{s}_{\mathrm{tr}}, \boldsymbol{s}_{\mathrm{re}}, \boldsymbol{s}_{\mathrm{rad}}) \leq 1 \ \forall \boldsymbol{\phi} \in \mathcal{F}$.

2) DISTURBANCE MODEL

Assume that $K_{\mathrm{tr,c}}$ and $K_{\mathrm{re,c}}$ clutter components are present in the transmissive and reflective half-spaces, respectively; then, $\boldsymbol{z}_{\mathrm{rad}}$ can be expanded as

$$\boldsymbol{z}_{\mathrm{rad}} = \sum_{k=1}^{K_{\mathrm{tr,c}}} \alpha_{\mathrm{tr,c},k} \gamma_{\mathrm{tr}}\big(\boldsymbol{\phi}_{\mathrm{tr,c},k}, \boldsymbol{s}_{\mathrm{tr}}, \boldsymbol{s}_{\mathrm{rad}}\big) \boldsymbol{h}\big(\boldsymbol{c}_{\mathrm{tr}}, \nu_{\mathrm{tr,c},k}\big) + \sum_{k=1}^{K_{\mathrm{re,c}}} \alpha_{\mathrm{re,c},k} \gamma_{\mathrm{re}}\big(\boldsymbol{\phi}_{\mathrm{re,c},k}, \boldsymbol{s}_{\mathrm{re}}, \boldsymbol{s}_{\mathrm{rad}}\big) \boldsymbol{h}\big(\boldsymbol{c}_{\mathrm{re}}, \nu_{\mathrm{re,c},k}\big) + \boldsymbol{w}_{\mathrm{rad}}, \quad (20)$$

where: $\boldsymbol{w}_{\mathrm{rad}}$ is a circularly-symmetric Gaussian random vector with covariance matrix $\sigma_{\mathrm{rad}}^2 \boldsymbol{I}_P$ accounting for the additive noise; $\alpha_{\mathrm{tr,c},k} \in \mathbb{C}$, $\nu_{\mathrm{tr,c},k} \in \mathbb{R}$, and $\boldsymbol{\phi}_{\mathrm{tr,c},k} \in \mathcal{F}_{\mathrm{tr,c}}$ are the complex amplitude, Doppler shift, and angular direction of the k-th clutter component in the transmissive half-space, respectively; $\alpha_{\mathrm{re,c},k} \in \mathbb{C}$, $\nu_{\mathrm{re,c},k} \in \mathbb{R}$, and $\boldsymbol{\phi}_{\mathrm{re,c},k} \in \mathcal{F}_{\mathrm{re,c}}$ are the complex amplitude, Doppler shift, and angular direction of the k-th clutter component in the reflective half-space, respectively. Here, $\mathcal{F}_{\mathrm{tr,c}} \subset \mathcal{F}_{\mathrm{tr}} \setminus \mathcal{F}_{\mathrm{tr,t}}$ and $\mathcal{F}_{\mathrm{re,c}} \subset \mathcal{F}_{\mathrm{re}} \setminus \mathcal{F}_{\mathrm{re,t}}$ are the angular regions containing the clutter components in the transmissive and reflective half-spaces, respectively, as depicted in Fig. 2; for future reference, we also define $\mathcal{F}_{\mathrm{c}} = \mathcal{F}_{\mathrm{tr,c}} \cup \mathcal{F}_{\mathrm{re,c}}$. Finally, we model $\alpha_{\mathrm{tr,c},k}$ and $\alpha_{\mathrm{re,c},k}$ as independent circularly-symmetric Gaussian random variables with variance $\sigma_{\mathrm{tr,c},k}^2$ and $\sigma_{\mathrm{re,c},k}^2$, respectively; accordingly, the disturbance covariance matrix is

$$\boldsymbol{C}_{\mathrm{rad}} = \sigma_{\mathrm{rad}}^2 \boldsymbol{I} + \sum_{k=1}^{K_{\mathrm{tr,c}}} \sigma_{\mathrm{tr,c},k}^2 |\gamma_{\mathrm{tr}}\big(\boldsymbol{\phi}_{\mathrm{tr,c},k}, \boldsymbol{s}_{\mathrm{tr}}, \boldsymbol{s}_{\mathrm{rad}}\big)|^2 \times \boldsymbol{h}\big(\boldsymbol{c}_{\mathrm{tr}}, \nu_{\mathrm{tr,c},k}\big) \boldsymbol{h}^{\mathsf{H}}\big(\boldsymbol{c}_{\mathrm{tr}}, \nu_{\mathrm{tr,c},k}\big) + \sum_{k=1}^{K_{\mathrm{re,c}}} \sigma_{\mathrm{re,c},k}^2 |\gamma_{\mathrm{re}}\big(\boldsymbol{\phi}_{\mathrm{re,c},k}, \boldsymbol{s}_{\mathrm{re}}, \boldsymbol{s}_{\mathrm{rad}}\big)|^2 \times \boldsymbol{h}\big(\boldsymbol{c}_{\mathrm{re}}, \nu_{\mathrm{re,c},k}\big) \boldsymbol{h}^{\mathsf{H}}\big(\boldsymbol{c}_{\mathrm{re}}, \nu_{\mathrm{re,c},k}\big). \quad (21)$$

C. USER RECEIVED SIGNAL

When the communication function is present, the STAR-RIS partitions the CPI into P/M time slots of equal duration, where M is chosen so that P/M is an integer and MT is smaller than the coherence time of the channel from the STAR-RIS to the user. In every time slot, the STAR-RIS sends two messages (one for each side) as discussed in Section III.

For illustration, consider the time slot $[0, MT]$ and the transmissive half-space. The signal received by the user is

$$y_{\mathrm{tr,u}}(t) = \sum_{k=1}^{K_{\mathrm{tr,u}}} \alpha_{\mathrm{tr,u},k}\varrho_{\mathrm{tr}}\big(t-\tau_{\mathrm{tr,u},k}, \boldsymbol{\phi}_{\mathrm{tr,u},k}\big) + z_{\mathrm{tr,\,u}}(t), \quad (22)$$

for $t \in [0, MT]$, where: $K_{\mathrm{tr,u}} \geq 1$ is the number of channel paths from the STAR-RIS to the user; $\alpha_{\mathrm{tr,u},k} \in \mathbb{C}$ is the amplitude of the k-th path; $\tau_{\mathrm{tr,u},k} \in [\tau_{\mathrm{tr,u,min}}, \tau_{\mathrm{tr,u,max}}]$ is the delay of the k-th path, with $0 \leq \tau_{\mathrm{tr,u,min}} \leq \tau_{\mathrm{tr,u,max}} \leq T-2\Delta$; $\boldsymbol{\phi}_{\mathrm{tr,u},k} \in \mathcal{F}_{\mathrm{tr,u}}$ is the angular direction of departure of the k-th path, with $\mathcal{F}_{\mathrm{tr,u}} \subset \mathcal{F}_{\mathrm{tr}}$; finally, $z_{\mathrm{tr,u}}(t)$ is the additive noise. The quantities $K_{\mathrm{tr,u}}$ and $\{\alpha_{\mathrm{tr,u},k}, \tau_{\mathrm{tr,u},k}, \phi_{\mathrm{tr,u},k}\}_{k=1}^{K_{\mathrm{tr,u}}}$ are unknown, as no instantaneous CSI is available. We only make the mild assumptions that the STAR-RIS knows the set $\mathcal{F}_{\mathrm{tr,u}}$ and the user knows the interval $[\tau_{\mathrm{tr,u,min}}, \tau_{\mathrm{tr,u,max}}]$; these quantities are tied to some prior information on the user location and can be enlarged at the design stage to account for greater uncertainty.

The signal in (22) is passed through a unit-energy filter matched to $\psi(t)$ and sampled at the Nyquist rate $1/B$. Upon denoting by $r_\psi(t) = \psi(t) * \psi^*(-t)$ the autocorrelation function of $\psi(t)$, the output samples are

$$\begin{aligned} y_{\mathrm{tr},u}(p,\ell) &= y_{\mathrm{tr,u}}(t) * \psi^*(-t)\,|_{t=\tau_{\mathrm{tr,u,min}}+pT+\ell/B} \\ &= c_{\mathrm{tr}}(p)\beta_{\mathrm{tr},u}(\ell) + z_{\mathrm{tr},u}(\ell,p), \end{aligned} \quad (23)$$

for $p = 0, \ldots, M-1$ and $\ell = 0, \ldots, L_{\mathrm{tr},u}-1$, where $L_{\mathrm{tr},u} = \lceil(\tau_{\mathrm{tr,u,max}} - \tau_{\mathrm{tr,u,min}} + 2\Delta)B\rceil$ and

$$\begin{aligned} \beta_{\mathrm{tr},u}(\ell) = \sum_{k=1}^{K_{\mathrm{tr,u}}} &\alpha_{\mathrm{tr,u},k}\sqrt{\mathcal{E}G_{\mathrm{ris}}\big(\boldsymbol{\phi}_{\mathrm{tr,u},k}\big)} \\ &\times r_\psi\big(\tau_{\mathrm{tr,u,min}} + \ell/B - \tau_{\mathrm{tr,u},k}\big) \\ &\times \big(\boldsymbol{u}_{\mathrm{ris}}^{\mathsf{T}}\big(\boldsymbol{\phi}_{\mathrm{tr,u},k}\big)\mathrm{diag}\{\boldsymbol{g}\}\boldsymbol{s}_{\mathrm{tr}}\big), \end{aligned} \quad (24a)$$

$$z_{\mathrm{tr},u}(p,\ell) = z_{\mathrm{tr,u}}(t) * \psi^*(-t)\,|_{t=\tau_{\mathrm{tr,u,min}}+pT+\ell/B}\,. \quad (24b)$$

The coefficients $\{\beta_{\mathrm{tr},u}(\ell)\}_{\ell=0}^{L_{\mathrm{tr},u}-1}$ are the tap amplitudes of the discrete-time channel from the feeder to the STAR-RIS to the user. Since $r_\psi(t) = 0$ if $|t| \geq \Delta$, the k-th channel path contributes to the ℓ-th channel tap in (24a) only if $|\tau_{\mathrm{tr,u,min}} + \ell/B - \tau_{\mathrm{tr,u},k}| < \Delta$, with a strength that depends on the spatial response of the STAR-RIS towards $\boldsymbol{\phi}_{\mathrm{tr,u},k}$. Finally, we model the noise samples $\{z_{\mathrm{tr},u}(\ell,p),\ \ell = 0, \ldots, L_{\mathrm{tr},u}-1,\ p = 0, \ldots, M-1\}$ are i.i.d. circularly-symmetric Gaussian random variables with variance σ_{com}^2.

For the reflective side, the signal received by the user is similarly derived: it is sufficient to replace the subscript "tr" with "re" in the above derivations from (22) to (24). For example, $K_{\mathrm{re,u}} \geq 1$ denotes the number of channel paths for the user in the reflective side, with the corresponding angles of departure belonging to the set $\mathcal{F}_{\mathrm{re,u}} \subset \mathcal{F}_{\mathrm{re}}$. For future reference, we also define $\mathcal{F}_{\mathrm{u}} = \mathcal{F}_{\mathrm{tr,u}} \cup \mathcal{F}_{\mathrm{re,u}}$.

III. SYSTEM DESIGN

The space-time response of the STAR-RIS, the analog beamformer of the radar receiver, and the implementation of the radar and communication receivers are under the control of the system engineer. In Section III-A, leveraging the knowledge of the channel $\boldsymbol{g}$ between the feeder and the STAR-RIS, we design the space response of the STAR-RIS and the analog beamformer of the radar receiver (namely, $\boldsymbol{s}_{\mathrm{tr}}$, $\boldsymbol{s}_{\mathrm{re}}$, and $\boldsymbol{s}_{\mathrm{rad}}$) to control the STAR-RIS array power pattern, the PESA array power pattern, and their product. In Section III-B, instead, we design the temporal response of the STAR-RIS (namely, $\boldsymbol{c}_{\mathrm{tr}}$ and $\boldsymbol{c}_{\mathrm{re}}$) to make the echoes received from the two half-spaces distinguishable by the radar receiver, while also conveying a message to the users in the absence of instantaneous CSI. Finally, in Section III-C, we discuss the implementation of the radar, which faces the challenge of a composite multiple hypotheses testing problem, and, in Section III-D, we design the communication receivers, which must to recover the encoded message in the absence of instantaneous CSI.

A. DESIGN OF $\boldsymbol{s}_{\mathrm{tr}}$, $\boldsymbol{s}_{\mathrm{re}}$, AND $\boldsymbol{s}_{\mathrm{rad}}$

Let $\bar{\mathcal{F}}_t$, $\bar{\mathcal{F}}_c$, and $\bar{\mathcal{F}}_u$ be the discrete sets containing a grid of angular directions taken from $\mathcal{F}_t$, $\mathcal{F}_c$, and $\mathcal{F}_u$, respectively. We consider the following design criterion

$$\begin{aligned} \max_{\boldsymbol{s}_{\mathrm{tr}},\boldsymbol{s}_{\mathrm{re}},\boldsymbol{s}_{\mathrm{rad}}} \quad & \sum_{\boldsymbol{\phi}\in\bar{\mathcal{F}}_{\mathrm{t}}} \mathrm{A}(\boldsymbol{\phi};\boldsymbol{s}_{\mathrm{tr}},\boldsymbol{s}_{\mathrm{re}},\boldsymbol{s}_{\mathrm{rad}}), \\ \text{s.t.} \quad & \mathrm{A}(\boldsymbol{\phi};\boldsymbol{s}_{\mathrm{tr}},\boldsymbol{s}_{\mathrm{re}},\boldsymbol{s}_{\mathrm{rad}}) \leq \zeta_c, \quad \forall\boldsymbol{\phi}\in\bar{\mathcal{F}}_{\mathrm{c}}, \\ & \mathrm{A}_{\mathrm{ris}}(\boldsymbol{\phi};\boldsymbol{s}_{\mathrm{tr}},\boldsymbol{s}_{\mathrm{re}}) \geq \zeta_u, \quad \forall\boldsymbol{\phi}\in\bar{\mathcal{F}}_{\mathrm{u}}, \\ & |s_{\mathrm{tr},n}| = |s_{\mathrm{re},n}| = 1, \quad n = 1,\ldots,N_{\mathrm{ris}}, \\ & |s_{\mathrm{rad},n}| = 1, \quad n = 1,\ldots,N_{\mathrm{rad}}, \end{aligned} \quad (25)$$

where $\zeta_c \in [0,1]$ and $\zeta_u \in [0,1]$ are design parameters. Problem (25) aims to obtain a large two-way array power pattern in the angular regions monitored by radar, while limiting the two-way array power pattern in the angular regions containing clutter (first constraint) and requiring a minimum value of the STAR-RIS array power pattern in the angular regions where the users are located (second constraint). The last two constraints ensure that the spatial beamformers of the STAR-RIS and the analog beamformer of the radar receiver have unit modulus entries (see Sections II-A and II-B, respectively). Only the knowledge of $\boldsymbol{g}$, $\mathcal{F}_{\mathrm{c}}$, and $\mathcal{F}_{\mathrm{u}}$ is required for this design criterion.

Since Problem (25) is non-convex, we derive a suboptimal solution by using to the augmented Lagrangian method with partial elimination of the constraints [45], [46]; the associated computations are provided in Appendix A. Finally note that, for a given region of interest $\mathcal{F}_{\mathrm{t}}$, the space response

of the STAR-RIS must be updated every time the radar transmitter to STAR-RIS channel $\boldsymbol{g}$, the set containing the angles of departure for the user channel path $\mathcal{F}_{\mathrm{u}}$, or the angular region containing the clutter components $\mathcal{F}_{\mathrm{c}}$ changes. This happens over a long time scale (at least P PRIs, the radar coherent processing interval) and does not significantly impact real-time operation. Additionally, the size of the sets $\mathcal{F}_u$ and $\mathcal{F}_c$ can be adjusted to meet the required complexity-performance tradeoff: smaller sets reduce the uncertainty and improve the system performance, but this requires more frequent updates of the STAR-RIS space response, which increases the computational burden.

B. DESIGN OF c_{tr} AND c_{re}

The temporal code sequences of the STAR-RIS must ensure that the echoes originated from different half-spaces can be distinguished [40]; therefore, $\boldsymbol{c}_{\mathrm{tr}}$ and $\boldsymbol{c}_{\mathrm{re}}$ should have a low cross-correlation and be Doppler tolerant. Also, any embedded message must be encoded by the STAR-RIS and decoded by the communication receiver in the absence of instantaneous CSI. Inspired by the frame-by-frame encoding rule in [47], we propose two encoding strategies, which result into a simultaneous or sequential illumination of the two half-spaces over a CPI. To proceed, assume that $P \geq 4$ is a power of 2 and that P/M is integer; accordingly, M is also a power of 2.

1) SIMULTANEOUS ILLUMINATION

The STAR-RIS operates here in the ES mode [19] and simultaneously illuminates both half-spaces in each PRI, i.e., $c_{\mathrm{tr}}(p), c_{\mathrm{re}}(p) \neq 0$ for $p = 0, \ldots, P-1$.

When the communication function is active, $\boldsymbol{c}_{\mathrm{tr}}$ and $\boldsymbol{c}_{\mathrm{re}}$ are constructed as the concatenation of P/M codewords taken from distinct codebooks $\mathcal{C}_{\mathrm{tr}}$ and $\mathcal{C}_{\mathrm{re}}$, respectively, so that $[\boldsymbol{c}_{\mathrm{tr}}]_{(m-1)M+1:mM} \in \mathcal{C}_{\mathrm{tr}}$ and $[\boldsymbol{c}_{\mathrm{re}}]_{(m-1)M+1:mM} \in \mathcal{C}_{\mathrm{re}}$, for $m = 1, \ldots, P/M$. Let $b \geq 1$ be the number of bits sent per time slot in each half-space also, let M be a power of two with $2^{b+1} \leq M \leq P$; finally, let $\boldsymbol{H}_M \in \{-1, 1\}^{M \times M}$ be the Hadamard of order M. Then, we propose to use the following codebooks

$$\mathcal{C}_{\mathrm{tr}} = \left\{\text{first } 2^b \text{ columns of } 1/\sqrt{2}\boldsymbol{H}_M\right\}, \tag{26a}$$

$$\mathcal{C}_{\mathrm{re}} = \left\{\text{last } 2^b \text{ columns of } 1/\sqrt{2}\boldsymbol{H}_M\right\}, \tag{26b}$$

where the factor $1/\sqrt{2}$ ensures that half of the energy is redirected in each half-space in every PRI. The transmission rate in each half-space is here $\mathcal{R} = \frac{b}{M}$ [bit per pulse]. Fig. 3 provides an illustration of this encoding rule, while Table 2 provides the possible values of M, b, and $\mathcal{R}$ when $P = 16$.

When the communication function is not active, $\boldsymbol{c}_{\mathrm{tr}}$ and $\boldsymbol{c}_{\mathrm{re}}$ are chosen as the first and last columns of $\boldsymbol{H}_P$, respectively, which corresponds to set $M = P$ and $b = 0$ in (26).

2) SEQUENTIAL ILLUMINATION

The STAR-RIS operates here in the TS mode [19] and illuminates the transmissive half-space in the subinterval $[0, PT/2)$ and the reflective half-space in $[PT/2, PT)$, i.e., we have $[\boldsymbol{c}_{\mathrm{tr}}]_{P/2+1:P} = [\boldsymbol{c}_{\mathrm{re}}]_{1:P/2} = \boldsymbol{0}_{P/2}$.

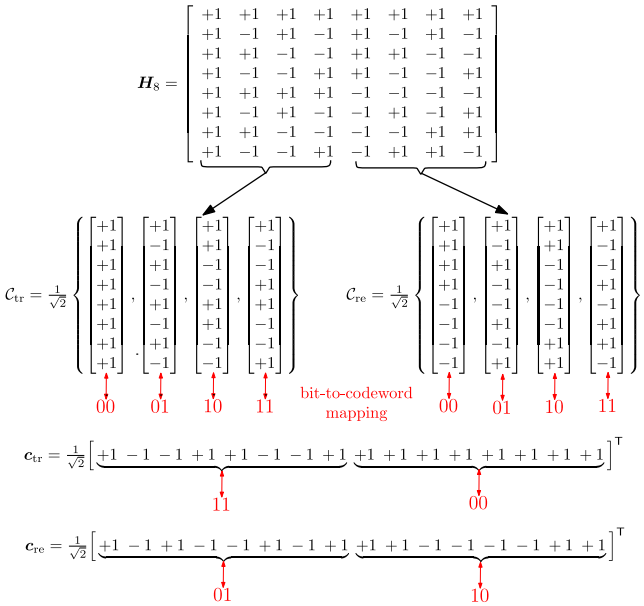

FIGURE 3. Encoding rule for simultaneous illumination when $P = 16$, $M = 8$, $b = 2$, and the bits 1100 and 0110 are sent in the transmissive and reflective half-spaces, respectively.

TABLE 2. Proposed encoding rules when $P = 16$.

M			
Simultaneous	Sequential	b	$\mathcal{R}$ [bit per pulse]
16	8	1	1/16
8	4	1	2/16
16	8	2	2/16
16	8	3	3/16
4	2	1	4/16
8	4	2	4/16

When the communication function is active, $[\boldsymbol{c}_{\mathrm{tr}}]_{1:P/2}$ and $[\boldsymbol{c}_{\mathrm{re}}]_{P/2+1:P}$ are constructed as the concatenation of $P/(2M)$ codewords taken from a codebook $\mathcal{C}$, so that $[\boldsymbol{c}_{\mathrm{tr}}]_{(m-1)M+1:mM} \in \mathcal{C}$ and $[\boldsymbol{c}_{\mathrm{re}}]_{P/2+(m-1)M+1:P/2+mM} \in \mathcal{C}$, for $m = 1, \ldots, P/(2M)$. Let $b \geq 1$ be the number of bits to be sent per time slot (either on the transmissive or the reflecting half-space); also, let M be a power of two with $2^b \leq M \leq P/2$. Then we use the following codebook

$$\mathcal{C} = \left\{\text{first } 2^b \text{ columns of } \boldsymbol{H}_M\right\}. \tag{27}$$

The transmission rate in each half-space is $\mathcal{R} = \frac{b}{2M}$ [bit per pulse], where the factor $1/2$ results from time splitting. Fig. 4 illustrates this encoding rule, while Table 2 reports the possible values of M, b, and $\mathcal{R}$ when $P = 16$.

When the communication function is not active, $[\boldsymbol{c}_{\mathrm{tr}}]_{1:P/2}$ and $[\boldsymbol{c}_{\mathrm{re}}]_{P/2+1:P}$ are both chosen as the first column of $\boldsymbol{H}_{P/2}$, which corresponds to set $M = P/2$ and $b = 0$ in (27).

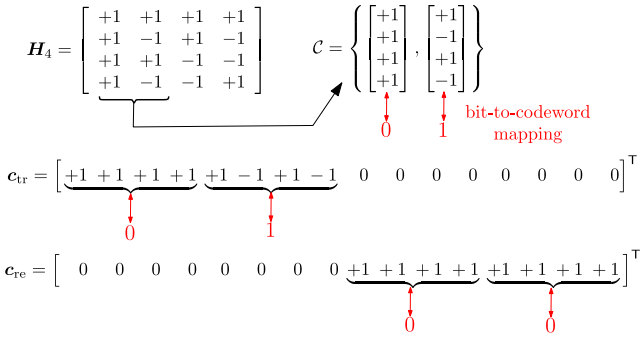

FIGURE 4. Encoding rule for sequential illumination when $P = 16$, $M = 4$, $b = 1$, and the bits 01 and 00 are sent in the transmissive and reflective half-spaces, respectively.

3) COMMENTS

Both encoding rules equally split the incident energy between the two half-spaces and, for a given P and b, can support the same transmission rate by arranging the value of M (see Table 2). In each time slot, the communication function relies on an orthogonal codebook to facilitate reliable message recovery at the communication receiver, as discussed in more detail later. Moreover, the P-dimensional code sequences $\boldsymbol{c}_{\rm tr}$ and $\boldsymbol{c}_{\rm re}$ resulting from the concatenation of P/M codewords are orthogonal irrespectively of the encoded message, which aids in separating echoes originating from different half-spaces in (16). As to this latter point, a distinction arises between simultaneous and sequential illuminations, which has implications for the radar receiver design. In sequential illumination, echoes from different half-spaces are orthogonal regardless of their Doppler shifts. In contrast, under simultaneous illumination, such echoes lose orthogonality when they exhibit different Doppler shifts.

Note that the proposed encoding schemes can work even in rapidly changing environments; for example, MT, which must be smaller than the channel coherence time, can be set as low as two PRIs in simultaneous illumination. The coefficients $c_{\rm tr}(p)$ and $c_{\rm re}(p)$ are updated once per PRI T. Since T is much larger than the inverse of the signal bandwidth, these updates occur at a significantly lower rate compared to the baseband sampling rate, making this operation lightweight for the STAR-RIS controller.

Finally, note that we are still making some idealistic assumptions to capture the STAR-RIS behavior in this study. In particular, we are using the phase-shift model, which, although widely adopted and convenient, is an oversimplified representation of the actual physical process [22]. Furthermore, we have adopted the common assumption that the phase shifts on the transmissive and reflective sides can be independently and continuously controlled. However, current hardware implementations can only support a finite set of reflection and transmission coefficients, and these coefficients are coupled [20], [22].

C. DESIGN OF THE RADAR RECEIVER

The radar detector relies on the knowledge of the code sequences $\boldsymbol{c}_{\rm tr}$ and $\boldsymbol{c}_{\rm re}$ to distinguish the echoes from different half-spaces. In particular, it is faced with a multiple composite hypotheses testing problem with four hypotheses:

- $\mathcal{H}_0$: no target is present in the cells under inspection;
- $\mathcal{H}_{1,\rm tr}$: a target with unknown amplitude and Doppler shift is present only in the transmissive cell;
- $\mathcal{H}_{1,\rm re}$: a target with unknown amplitude and Doppler shift is present only in the reflective cell;
- $\mathcal{H}_2$: a target with unknown amplitude and Doppler shift is present in each resolution cell under inspection.

Since this problem can be regarded as a model order selection, we propose to use a GIC-based decision rule [42]; hence, the selected hypothesis is

$$\hat{\mathcal{H}} = \underset{\mathcal{L}\in\{\mathcal{H}_0,\mathcal{H}_{1,\rm tr},\mathcal{H}_{1,\rm re},\mathcal{H}_2\}}{\arg\max}\ \mu(\mathcal{L}), \tag{28}$$

where

$$\mu(\mathcal{L}) = \begin{cases} f_{\mathcal{H}_0}\big(\boldsymbol{y}_{\rm rad}\big), & \text{if } \mathcal{L}=\mathcal{H}_0, \\ \max\limits_{\substack{\alpha_{\rm tr,t}\in\mathbb{C}\\ \nu_{\rm tr,t}\in\mathcal{V}_{\rm tr,t}}} \big\{f_{\mathcal{H}_{1,\rm tr}}\big(\boldsymbol{y}_{\rm rad};\alpha_{\rm tr,t},\nu_{\rm tr,t}\big)-\eta_{\rm rad}\big\}, & \text{if } \mathcal{L}=\mathcal{H}_{1,\rm tr}, \\ \max\limits_{\substack{\alpha_{\rm re,t}\in\mathbb{C}\\ \nu_{\rm re,t}\in\mathcal{V}_{\rm re,t}}} \big\{f_{\mathcal{H}_{1,\rm re}}\big(\boldsymbol{y}_{\rm rad};\alpha_{\rm re,t},\nu_{\rm re,t}\big)-\eta_{\rm rad}\big\}, & \text{if } \mathcal{L}=\mathcal{H}_{1,\rm re}, \\ \max\limits_{\substack{\boldsymbol{\alpha}_{\rm t}\in\mathbb{C}^2\\ \boldsymbol{\nu}_{\rm t}\in\mathcal{V}_{\rm tr,t}\times\mathcal{V}_{\rm re,t}}} \big\{f_{\mathcal{H}_2}\big(\boldsymbol{y}_{\rm rad};\boldsymbol{\alpha}_{\rm t},\boldsymbol{\nu}_{\rm t}\big)-2\eta_{\rm rad}\big\}, & \text{if } \mathcal{L}=\mathcal{H}_2, \end{cases} \tag{29}$$

$f_{\mathcal{L}}(\boldsymbol{y}_{\rm rad};\cdot)$ is the log-likelihood function under $\mathcal{L}$, $\boldsymbol{\alpha}_{\rm t} = [\alpha_{\rm tr,t};\alpha_{\rm re,t}]$, $\boldsymbol{\nu}_{\rm t} = [\nu_{\rm tr,t};\nu_{\rm re,t}]$, $\mathcal{V}_{\rm tr,t}$ and $\mathcal{V}_{\rm re,t}$ are the Doppler search intervals in the transmissive and reflective half-space, respectively, and $\eta_{\rm rad}$ is a penalty factor that can be set to control the false alarm rate under $\mathcal{H}_0$.

To proceed, define the following quantities:

$$\boldsymbol{\xi}_{\rm tr}\big(\nu_{\rm tr,t}\big) = \boldsymbol{C}_{\rm rad}^{-1}\boldsymbol{h}\big(\boldsymbol{c}_{\rm tr},\nu_{\rm tr,t}\big)/\|\boldsymbol{C}_{\rm rad}^{-\frac{1}{2}}\boldsymbol{h}\big(\boldsymbol{c}_{\rm tr},\nu_{\rm tr,t}\big)\|, \tag{30a}$$

$$\boldsymbol{\xi}_{\rm re}\big(\nu_{\rm re,t}\big) = \boldsymbol{C}_{\rm rad}^{-1}\boldsymbol{h}\big(\boldsymbol{c}_{\rm re},\nu_{\rm re,t}\big)/\|\boldsymbol{C}_{\rm rad}^{-\frac{1}{2}}\boldsymbol{h}\big(\boldsymbol{c}_{\rm re},\nu_{\rm re,t}\big)\|, \tag{30b}$$

$$\boldsymbol{\Xi}(\boldsymbol{\nu}_{\rm t}) = \boldsymbol{C}_{\rm rad}^{-1}\boldsymbol{H}_{\rm rad}(\boldsymbol{\nu}_{\rm t}) \times\big(\boldsymbol{H}_{\rm rad}^{\rm H}(\boldsymbol{\nu}_{\rm t})\boldsymbol{C}_{\rm rad}^{-1}\boldsymbol{H}_{\rm rad}(\boldsymbol{\nu}_{\rm t})\big)^{-1/2}, \tag{30c}$$

where $\boldsymbol{H}_{\rm rad}(\boldsymbol{\nu}_{\rm t}) = \big[\boldsymbol{h}(\boldsymbol{c}_{\rm re},\nu_{\rm re,t})\ \boldsymbol{h}(\boldsymbol{c}_{\rm tr},\nu_{\rm tr,t})\big]$. Then, upon exploiting the fact that the disturbance is Gaussian and after some elaborations, the rule in (28) can be recast as [48], [49]

$$\hat{\mathcal{H}} = \underset{\mathcal{L}\in\{\mathcal{H}_0,\mathcal{H}_{1,\rm tr},\mathcal{H}_{1,\rm re},\mathcal{H}_2\}}{\arg\max}\ \bar{\mu}(\mathcal{L}), \tag{31}$$

where

$$\bar{\mu}(\mathcal{L}) = \begin{cases} 0, & \text{if } \mathcal{L}=\mathcal{H}_0, \\ \max\limits_{\nu_{\rm tr,t}\in\mathcal{V}_{\rm tr,t}} \Big\{\Big|\boldsymbol{\xi}_{\rm tr}^{\rm H}\big(\nu_{\rm tr,t}\big)\boldsymbol{y}_{\rm rad}\Big|^2-\eta_{\rm rad}\Big\}, & \text{if } \mathcal{L}=\mathcal{H}_{1,\rm tr}, \\ \max\limits_{\nu_{\rm re,t}\in\mathcal{V}_{\rm re,t}} \Big\{\Big|\boldsymbol{\xi}_{\rm re}^{\rm H}\big(\nu_{\rm re,t}\big)\boldsymbol{y}_{\rm rad}\Big|^2-\eta_{\rm rad}\Big\}, & \text{if } \mathcal{L}=\mathcal{H}_{1,\rm re}, \\ \max\limits_{\boldsymbol{\nu}_{\rm t}\in\mathcal{V}_{\rm tr,t}\times\mathcal{V}_{\rm re,t}} \Big\{\Big\|\boldsymbol{\Xi}^{\rm H}(\boldsymbol{\nu}_{\rm t})\boldsymbol{y}_{\rm rad}\Big\|^2 -2\eta_{\rm rad}\Big\}, & \text{if } \mathcal{L}=\mathcal{H}_2. \end{cases} \tag{32}$$

When a target is detected, an estimate of its Doppler shift (and hence radial velocity) is provided by the maximizer of the objective function in (32) under $\hat{\mathcal{H}}$.

Remark 3: The matrix $\boldsymbol{C}_{\text{rad}}$ in (21) is data-dependent, and its computation and inversion must be performed for each CPI; this entails a computational complexity of $\mathcal{O}((K_{\text{tr,c}}+K_{\text{re,c}})(P^2+N_{\text{rad}}+N_{\text{ris}})+P^3)$. The evaluation of the quantities in (30), for all $[\nu_{\text{tr,t}};\nu_{\text{re,t}}]\in\mathcal{V}_{\text{tr,t}}\times\mathcal{V}_{\text{re,t}}$, has a cost of $\mathcal{O}(|\mathcal{V}_{\text{tr,t}}||\mathcal{V}_{\text{re,t}}|P^2)$. The computational complexity of the GIC-based rule in (31) is, therefore, $\mathcal{O}((K_{\text{tr,c}}+K_{\text{re,c}})(P^2+N_{\text{rad}}+N_{\text{ris}})+P^3+|\mathcal{V}_{\text{tr,t}}||\mathcal{V}_{\text{re,t}}|P^2)$. If clutter can be mitigated by properly designing the two-way array power pattern, we can assume $\boldsymbol{C}_{\text{rad}}\simeq\sigma^2_{\text{rad}}\boldsymbol{I}_P$ at the design stage: this simplifies the implementation of the radar receiver and eliminates the need for prior knowledge of the clutter parameters. The computational cost of this reduced-complexity decision rule is $\mathcal{O}(|\mathcal{V}_{\text{tr,t}}||\mathcal{V}_{\text{re,t}}|P^2)$.

Remark 4: The implementation of the rule in (31) simplifies for sequential illumination. To verify this, let $\bar{\boldsymbol{y}}_{\text{rad}}\in\mathbb{C}^{P/2}$ and $\underline{\boldsymbol{y}}_{\text{rad}}\in\mathbb{C}^{P/2}$ be the vectors containing the first and the last half entries of $\boldsymbol{y}_{\text{rad}}$, respectively. Notice that, since the last half entries of $\boldsymbol{h}(\boldsymbol{c}_{\text{tr}},\nu_{\text{tr,t}})$ and the first half entries of $\boldsymbol{h}(\boldsymbol{c}_{\text{re}},\nu_{\text{re,t}})$ are zeros for sequential illumination, $\bar{\boldsymbol{y}}_{\text{rad}}$ and $\underline{\boldsymbol{y}}_{\text{rad}}$ only contain echoes originated from the transmissive and reflective half-spaces, respectively. Consequently, the solution in (31) can equivalently be obtained by running two independent binary tests, one for each half-space, namely,

$$\max_{\nu_{\text{tr,t}}\in\mathcal{V}_{\text{tr,t}}}\left|\bar{\boldsymbol{\xi}}^{\mathsf{H}}_{\text{tr}}(\nu_{\text{tr,t}})\bar{\boldsymbol{y}}_{\text{rad}}\right|^2\underset{\mathcal{H}^{\text{seq}}_{0,\text{tr}}}{\overset{\mathcal{H}^{\text{seq}}_{1,\text{tr}}}{\gtrless}}\eta_{\text{rad}},\tag{33a}$$

$$\max_{\nu_{\text{re,t}}\in\mathcal{V}_{\text{re},t}}\left|\underline{\boldsymbol{\xi}}^{\mathsf{H}}_{\text{re}}(\nu_{\text{re,t}})\underline{\boldsymbol{y}}_{\text{rad}}\right|^2\underset{\mathcal{H}^{\text{seq}}_{0,\text{re}}}{\overset{\mathcal{H}^{\text{seq}}_{1,\text{re}}}{\gtrless}}\eta_{\text{rad}},\tag{33b}$$

where $\bar{\boldsymbol{\xi}}_{\text{tr}}(\nu_{\text{tr,t}})\in\mathbb{C}^{P/2}$ contains the first half entries of $\boldsymbol{\xi}_{\text{tr}}(\nu_{\text{tr,t}})$, while $\underline{\boldsymbol{\xi}}_{\text{re}}(\nu_{\text{re,t}})\in\mathbb{C}^{P/2}$ the last half entries of $\boldsymbol{\xi}_{\text{re}}(\nu_{\text{re,t}})$; then, a decision $\hat{\mathcal{H}}$ is taken as follows:

- $\mathcal{H}_0$ is declared if $\mathcal{H}^{\text{seq}}_{0,\text{tr}}$ and $\mathcal{H}^{\text{seq}}_{0,\text{re}}$ are true;
- $\mathcal{H}_{1,\text{tr}}$ is declared if $\mathcal{H}^{\text{seq}}_{1,\text{tr}}$ and $\mathcal{H}^{\text{seq}}_{0,\text{re}}$ are true;
- $\mathcal{H}_{1,\text{re}}$ is declared if $\mathcal{H}^{\text{seq}}_{0,\text{tr}}$ and $\mathcal{H}^{\text{seq}}_{1,\text{re}}$ are true;
- $\mathcal{H}_2$ is declared if $\mathcal{H}^{\text{seq}}_{1,\text{tr}}$ and $\mathcal{H}^{\text{seq}}_{1,\text{re}}$ are true.

The joint Doppler search under $\mathcal{H}_2$ is now avoided. Also, the involved vectors and matrices have smaller size: for example, $\bar{\boldsymbol{\xi}}_{\text{tr}}(\nu_{\text{tr,t}})=\bar{\boldsymbol{C}}^{-1}_{\text{rad}}\bar{\boldsymbol{h}}(\boldsymbol{c}_{\text{tr}},\nu_{\text{tr,t}})/\|\bar{\boldsymbol{C}}^{-1/2}_{\text{rad}}\bar{\boldsymbol{h}}(\boldsymbol{c}_{\text{tr}},\nu_{\text{tr,t}})\|$, where $\bar{\boldsymbol{h}}(\boldsymbol{c}_{\text{tr}},\nu_{\text{tr,t}})$ contains the first half entries of $\boldsymbol{h}(\boldsymbol{c}_{\text{tr}},\nu_{\text{tr,t}})$ and $\bar{\boldsymbol{C}}_{\text{rad}}$ is the principal submatrix of $\boldsymbol{C}_{\text{rad}}$ obtained by deleting the last $P/2$ rows and the last $P/2$ columns. The computational complexity in this case is $\mathcal{O}((K_{\text{tr,c}}+K_{\text{re,c}})(P^2+N_{\text{rad}}+N_{\text{ris}})+P^3+(|\mathcal{V}_{\text{tr,t}}|+|\mathcal{V}_{\text{re,t}}|)P^2)$ and can be reduced to $\mathcal{O}((|\mathcal{V}_{\text{tr,t}}|+|\mathcal{V}_{\text{re,t}}|)P^2)$, if clutter is mitigated by properly designing the two-way array power pattern (see Remark 3).

D. DESIGN OF THE COMMUNICATION RECEIVER

Without loss of generality, assume simultaneous illumination and consider the user in the transmissive half-space: the same discussion applies for sequential illumination and/or for the user in the reflective half-space. To recover the codeword $[\boldsymbol{c}_{\text{tr}}]_{1:M}\in\mathcal{C}_{\text{tr}}$ from the measurements in (23), we resort to a ML decoder combined with a GIC-based rule to estimate the number of channel taps with non-zero amplitude [42].

For each $\boldsymbol{c}\in\mathcal{C}_{\text{tr}}$, define

$$T_{\text{tr}}(\boldsymbol{c},\ell)=\frac{1}{\|\boldsymbol{c}\|^2}\left|\sum_{p=1}^{M}c^*(p)y_{\text{tr},u}(p,\ell)\right|^2,\tag{34}$$

for $\ell=0,\ldots,L_{\text{tr},u}-1$, and

$$\hat{\ell}(\boldsymbol{c})=\underset{\ell=0,\ldots,L_{\text{tr},u}-1}{\arg\max}\ T_{\text{tr}}(\boldsymbol{c},\ell).\tag{35}$$

Then, as shown in Appendix B, an estimate of the transmitted codeword is

$$\hat{\boldsymbol{c}}=\underset{\boldsymbol{c}\in\mathcal{C}_{\text{tr}}}{\arg\max}\left\{\ T_{\text{tr}}\Big(\boldsymbol{c},\hat{\ell}(\boldsymbol{c})\Big)+\sum_{\ell=1,\ \ell\neq\hat{\ell}(\boldsymbol{c})}^{L_{\text{tr},u}}\big(T_{\text{tr}}(\boldsymbol{c},\ell)-\eta_{\text{com}}\big)^+\right\},\tag{36}$$

where $\eta_{\text{com}}\geq 0$ is a threshold that can be set so as to avoid using those measurements corresponding to channel taps that are weak (and therefore less reliable) or contain only noise. Here, we propose to select η_{com} to have a desired probability that the energy of a noise-only channel tap exceeds η_{com}, i.e., to have $\Pr(T_{\text{tr}}(\boldsymbol{c},\ell)>\eta_{\text{com}}|\ \beta_{\text{tr},u}(\ell)=0)=\epsilon_{\text{com}}$. Since $T_{\text{tr}}(\boldsymbol{c},\ell)$ is an exponential random variable with mean value σ^2_{com} when $\beta_{\text{tr},u}(\ell)=0$, we obtain $\eta_{\text{com}}=\sigma^2_{\text{com}}\ln(1/\epsilon_{\text{com}})$. Observe that this receiver is quite simple. Indeed, the computational cost for evaluating the statistics in (34), for all $\boldsymbol{c}\in\mathcal{C}_{\text{tr}}$ and $\ell\in\{0,\ldots,L_{\text{tr},u}\}$, is $\mathcal{O}(L_{\text{tr},u}|\mathcal{C}_{\text{tr}}|M)$. Since $|\mathcal{C}_{\text{tr}}|=2^b\leq M$, the computational complexity of the GIC-based rule in (36) is $\mathcal{O}(L_{\text{tr},u}M^2)$.

IV. PERFORMANCE ANALYSIS

We provide here some numerical examples to assess the radar and communication performance.

A. PARAMETER SETTING

The main system parameters are summarized in Table 3. The feeder employs rectangular pulses. The STAR-RIS and the radar receiving array have a square structure with half-wavelength element spacing, and their element gain is modeled as $G_{\text{ris}}(\boldsymbol{\phi})=G_{\text{rad}}(\boldsymbol{\phi})=\pi/4\cos^2\phi^{\text{az}}\cos^2\phi^{\text{el}}$. The feeder and STAR-RIS are in each other's far field, and the corresponding channel is modeled as

$$\boldsymbol{g}=\left(\frac{G_{\text{f}}G_{\text{ris}}(\boldsymbol{\phi}_{\text{f}})\lambda^2}{(4\pi)^2d_{\text{f}}^2}\right)^{\frac{1}{2}}\boldsymbol{u}_{\text{ris}}(\boldsymbol{\phi}_{\text{f}}),\tag{37}$$

TABLE 3. System parameters.

f_o	Carrier frequency	28 GHz
B	Bandwidth	50 MHz
$\mathcal{P}$	Pulse Power	30 dBm
T	Pulse repetition interval (PRI)	0.25 ms
P	Number of PRIs	16
$N_{\rm ris}$	Number of STAR-RIS elements	16×16
$N_{\rm rad}$	Number of radar PESA elements	16×16
$\mathcal{V}_{\rm tr,t}$	Target Doppler interval (tr. side)	$(1.75\,\text{kHz}, 2\,\text{kHz})$
$\mathcal{V}_{\rm re,t}$	Target Doppler interval (re. side)	$(0.25\,\text{kHz}, 0.5\,\text{kHz})$
$\mathcal{V}_{\rm tr,c}$	Clutter Doppler interval (tr. side)	$(-0.25\,\text{kHz}, 0.25\,\text{kHz})$
$\mathcal{V}_{\rm re,c}$	Clutter Doppler interval (re. side)	$(-0.25\,\text{kHz}, 0.25\,\text{kHz})$
$\mathcal{F}_{\rm tr,t}$	Target angular region (tr. side)	$(-2^\circ, 2^\circ) \times (-2^\circ, 2^\circ)$
$\mathcal{F}_{\rm re,t}$	Target angular region (re. side)	$(178^\circ, 182^\circ) \times (-2^\circ, 2^\circ)$
$\mathcal{F}_{\rm tr,c}$	Clutter angular region (tr. side)	$(202^\circ, 238^\circ) \times (-4^\circ, 4^\circ)$
$\mathcal{F}_{\rm re,c}$	Clutter angular region (re. side)	$(-4^\circ, 4^\circ) \times (-58^\circ, -22^\circ)$
$\mathcal{F}_{\rm tr,u}$	User angular region (tr. side)	$(138^\circ, 142^\circ) \times (-42^\circ, -38^\circ)$
$\mathcal{F}_{\rm re,u}$	User angular region (re. side)	$(-42^\circ, -38^\circ) \times (-12^\circ, -8^\circ)$
$\sigma^2_{\rm rad}$	Noise power spectral density	-164 dBm/Hz

where $G_{\rm f} = 20$ dB is the antenna gain of the feeder and $d_{\rm f} = 3$ m and $\boldsymbol{\phi}_{\rm f} = [-45^\circ; 0^\circ]$ are the distance and the angular direction of the feeder from the STAR-RIS, respectively.

As to the radar, the unambiguous Doppler interval is $(-1/(2T), 1/(2T))$, where $1/(2T) = 2$ kHz corresponds to a radial velocity of about 10.7 m/s, while the Doppler resolution is $1/(PT) = 250$ kHz, corresponding to a radial velocity of about 1.3 m/s for $P = 16$ [50]; finally, we set $\zeta_{\rm c} = -60$ dB in Problem (25), while $\eta_{\rm rad}$ is chosen to have an average number of false alarms of 10^{-4} under $\mathcal{H}_0$ in the implementation of the GLRT. As to the targets, the directions $\boldsymbol{\phi}_{\rm tr,t}$ and $\boldsymbol{\phi}_{\rm re,t}$ are uniformly sampled from $\mathcal{F}_{\rm tr,t}$ and $\mathcal{F}_{\rm re,t}$, respectively; also, the Doppler shifts $\nu_{\rm tr,t}$ and $\nu_{\rm re,t}$ are uniformly sampled from $\mathcal{V}_{\rm tr,t}$ and $\mathcal{V}_{\rm re,t}$, respectively; finally, a Swerling I fluctuation is considered, and the amplitudes $\alpha_{\rm tr,t}$ and $\alpha_{\rm re,t}$ are generated as independent realizations of a circularly-symmetric complex Gaussian variable with variance

$$\sigma_{\rm t}^2 = \frac{\text{RCS}_{\rm t}}{(4\pi)^2 d_{\rm rad}^4}, \tag{38}$$

where $\text{RCS}_{\rm t}$ is the target radar cross-section and $d_{\rm rad} = 10$ m is the range under inspection. As to the clutter, we assume $K_{\rm tr,\,c} = K_{\rm re,\,c} = K_{\rm c}$, with $K_{\rm c} = 95$; $\{\boldsymbol{\phi}_{{\rm tr,c},k}\}_{k=1}^{K_{\rm c}}$ and $\{\boldsymbol{\phi}_{{\rm re,c},k}\}_{k=1}^{K_{\rm c}}$ are uniformly sampled from $\mathcal{F}_{\rm tr,c}$ and $\mathcal{F}_{\rm re,c}$, respectively; $\{\nu_{{\rm tr,c},k}\}_{k=1}^{K_{\rm c}}$ and $\{\nu_{{\rm re,c},k}\}_{k=1}^{K_{\rm c}}$ are uniformly sampled from $\mathcal{V}_{\rm tr,c}$ and $\mathcal{V}_{\rm re,c}$, respectively; finally,

$$\sigma_{{\rm tr,c},k}^2 = \sigma_{{\rm re,c},k}^2 = \frac{\text{RCS}_{\rm c}}{(4\pi)^2 d_{\rm rad}^4}, \tag{39}$$

where $\text{RCS}_{\rm c} = 15$ dBsm is the clutter radar cross-section.

At the communication receiver, we set $\epsilon_{\rm com} = 10^{-2}$. As to the users, we assume $L_{\rm tr,\,u} = L_{\rm re,\,u} = L_{\rm u}$, $K_{\rm tr,\,u} = K_{\rm re,\,u} = K_{\rm u}$, with $L_{\rm u} = 15$ and $K_{\rm u} = 3$; $\{\tau_{{\rm tr,u},k}, \tau_{{\rm re,u},k}\}_{k=1}^{K_{\rm u}}$ are uniformly sampled from $\{\tau_{\rm tr,u,min} + \ell/B\}_{\ell=0}^{L_{\rm u}-1}$; $\{\boldsymbol{\phi}_{{\rm tr,u},k}\}_{k=1}^{K_{\rm u}}$ and $\{\boldsymbol{\phi}_{{\rm re,u},k}\}_{k=1}^{K_{\rm u}}$ are uniformly sampled from $\mathcal{F}_{\rm tr,u}$ and $\mathcal{F}_{\rm re,u}$, respectively; Rayleigh fading is considered, and $\{\alpha_{{\rm tr,u},k}, \alpha_{{\rm re,u},k}\}_{k=1}^{K_{\rm u}}$ are generated as independent realizations of a circularly-symmetric complex Gaussian variable with variance $\sigma_{\rm u}^2$; finally, for future reference, we define the communication SNR as

$$\text{SNR}_{\rm com} = \frac{\mathcal{E} G_{\rm ris}(\mathbf{0}_2) \|\boldsymbol{g}\|_1^2 \sigma_u^2 \zeta_{\rm u} K_{\rm u}}{L_{\rm u} \sigma_{\rm com}^2}. \tag{40}$$

B. PERFORMANCE METRICS

For the radar function, we evaluate the probability of detection (PD), defined here as the probability of correctly declaring hypothesis $\mathcal{H}_2$ when it is true, and the RMSE in estimating the target's radial velocity. For the communication function, we consider the BER, averaged across both users. These performance metrics are analyzed with respect to the following parameters: the target's radar cross-section ($\text{RCS}_{\rm t}$), the communication signal-to-noise ratio ($\text{SNR}_{\rm com}$), the maximum value of the STAR-RIS array power pattern in the angular regions corresponding to the users (ζ_u), and the data encoding schemes in Table 2.

Regarding radar performance, note that the test statistics in (33) is independent of the message transmitted to the users. Specifically, conditioned on $\alpha_{\rm tr,t}$, $2|\bar{\boldsymbol{\xi}}_{\rm tr}^{\rm H}(\nu_{\rm tr,t})\bar{\boldsymbol{y}}_{\rm rad}|^2$ follows an exponential distribution with mean 1 under $\mathcal{H}_{0,{\rm tr}}^{\rm seq}$, and a noncentral chi-squared distribution with 2 degrees of freedom and noncentrality parameter

$$2|\alpha_{\rm tr,t}|^2 |\gamma_{\rm tr}(\boldsymbol{\phi}_{\rm tr,t}; \boldsymbol{s}_{\rm tr}, \boldsymbol{s}_{\rm rad})|^2 \bar{\boldsymbol{d}}^{\rm H}(\nu_{\rm tr,t}) \left(\sigma_{\rm rad}^2 \boldsymbol{I}_{P/2} + \sum_{k=1}^{K_{\rm tr,c}} \sigma_{{\rm tr,c},k}^2 |\gamma_{\rm tr}(\boldsymbol{\phi}_{{\rm tr,c},k}, \boldsymbol{s}_{\rm tr}, \boldsymbol{s}_{\rm rad})|^2 \times \bar{\boldsymbol{d}}(\nu_{{\rm tr,c},k}) \bar{\boldsymbol{d}}^{\rm H}(\nu_{{\rm tr,c},k}) \right)^{-1} \bar{\boldsymbol{d}}(\nu_{\rm tr,t}), \tag{41}$$

under $\mathcal{H}_{1,{\rm tr}}^{\rm seq}$, where $\bar{\boldsymbol{d}}(\nu) = [1; {\rm e}^{{\rm i}2\pi T\nu}; \cdots; {\rm e}^{{\rm i}2\pi\nu T(P/2-1)}]$. The same reasoning applies to $2|\bar{\boldsymbol{\xi}}_{\rm re}^{\rm H}(\nu_{\rm re,t})\bar{\boldsymbol{y}}_{\rm rad}|^2$. As a result, in the case of sequential illumination, radar performance is unaffected by the communication data (a desirable property). In contrast, for simultaneous illumination, radar performance generally depends on the data, although, as shown in the next subsection, this dependency is relatively weak.

Regarding communication performance, conditioned on $\{\beta_{{\rm tr},u}(\ell)\}_{\ell=0}^{L_{{\rm tr},u}-1}$, the statistics in (34) are independent. In particular, the quantity $(2/\sigma_{\rm com}^2) T_{\rm tr}(\boldsymbol{c}, \ell)$ follows a noncentral chi-squared distribution with two degrees of freedom and noncentrality parameter $2\|\boldsymbol{c}_{\rm tr}\|^2 |\beta_{{\rm tr},u}(\ell)|^2 / \sigma_{\rm com}^2$, if $\boldsymbol{c} = \boldsymbol{c}_{\rm tr}$ and $\beta_{{\rm tr},u}(\ell) \neq 0$. Otherwise, it follows an exponential distribution with mean 1. This implies that the BER depends solely on the number of the codewords and their energy. Consequently, for a given b (i.e., a given codebook size), the communication performance for simultaneous and sequential illumination is identical if the codeword length M in the former is set to twice the value used in the latter: an arrangement that is satisfied for each row of Table 2 and that also ensures a common transmission rate.

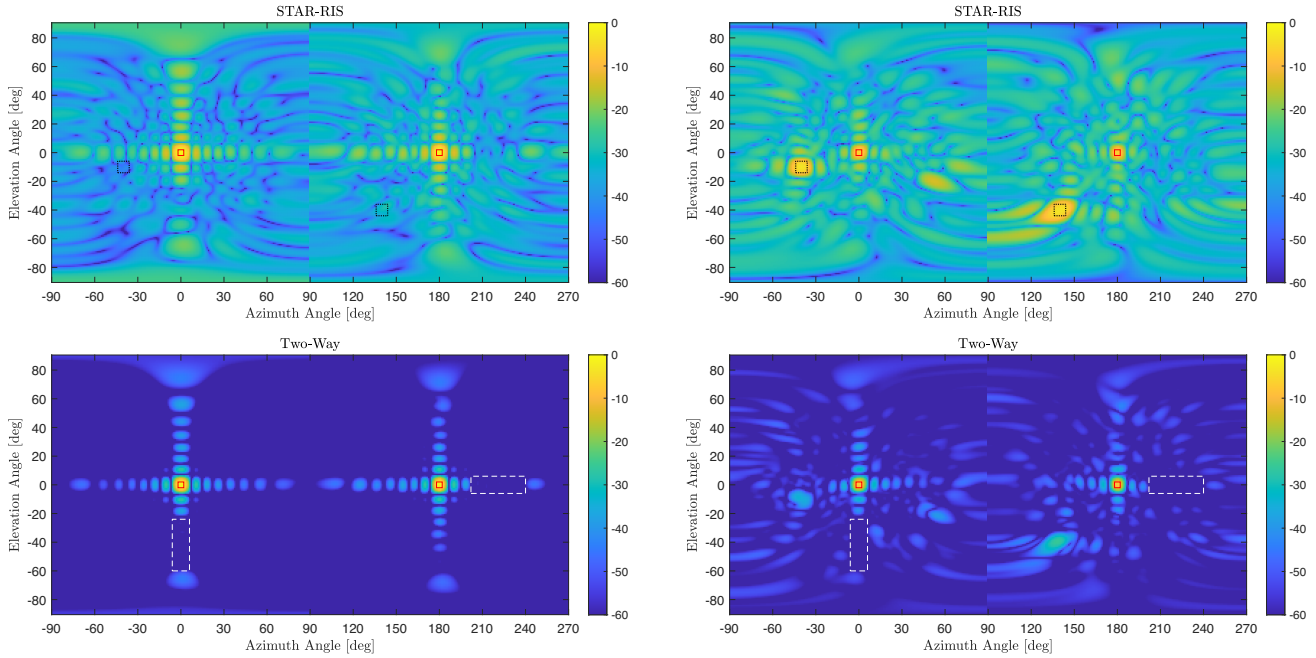

(a) $\zeta_u = -\infty$ (b) $\zeta_u = -5$ dB

FIGURE 5. STAR-RIS (top) and two-way (bottom) array power patterns for $\zeta_u = -\infty$ (left) and $\zeta_u = -5$ dB (right). Red solid-line squares indicate the target regions; black dotted-line squares indicate the user regions; white dashed-line rectangles indicate the clutter regions.

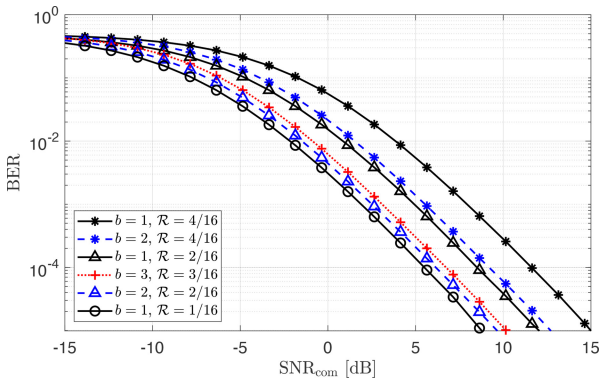

FIGURE 6. BER vs the communication SNR for simultaneous and sequential illumination and for different $(b, \mathcal{R})$ pairs when $\zeta_u = -5$ dB and $\zeta_c = -60$ dB.

C. NUMERICAL RESULTS

We first analyze the ability to control the transmit and receive array response. Figure 5 shows the STAR-RIS and two-way array power patterns obtained by solving Problem (25) for $\zeta_u = -\infty$ (the users' constraints are not active) and $\zeta_u = -5$ dB (the users' constraints are active). When $\zeta_u = -\infty$, the STAR-RIS array power pattern only contains one sharp beam in each half-space that points towards the prospective target. Instead, for $\zeta_u = -5$ dB, the STAR-RIS forms two beams in each half-space that points towards both the prospective target and the user, thus safeguarding the communication performance. In both cases, the two-way array power pattern only present one a sharp beam in each half-space, pointing towards the prospective target, and its sidelobes remain below -60 dB in the cluttered region $\mathcal{F}_c$.

Next, we evaluate the impact of the proposed encoding rules on the system performance under the condition $\zeta_u = -5$ dB. Fig. 6 presents BER versus SNR$_{com}$ for all cases listed in Table 2. Recall that, when $b = 1$, a transmission rate of $1/16$ is achieved by setting $M = 16$ for simultaneous illumination and $M = 8$ for sequential illumination. As discussed in Section IV-B, both configurations yield identical BER performance. A similar observation holds for the other $(b, \mathcal{R})$ pairs reported in Table 2. Fig. 7 presents PD and RMSE versus RCS$_t$ for both simultaneous and sequential illumination schemes. For sequential illumination, radar performance is independent of the specific $(b, \mathcal{R})$ pair, as discussed in Section IV-B. For simultaneous illumination, instead, we consider for illustration the two extreme cases in Fig. 6, namely, $(b, \mathcal{R}) = (1, 4/16)$ and $(b, \mathcal{R}) = (1, 1/16)$. We also include the performance of a radar-only system, optimized for radar functionality by setting $\zeta_u = -\infty$. Several key observations can be made.

- *Communication Trade-offs.* Fig. 6 shows that different trade-offs between transmission rate and error performance can be achieved. For a fixed b (or equivalently, a fixed $\mathcal{R}$), the BER decreases as $\mathcal{R}$ decreases (or b increases). This is because the codeword length M increases, which in turn increases the received signal energy. For example, when comparing the extreme cases $(b, \mathcal{R}) = (1, 4/16)$ and $(b, \mathcal{R}) = (1, 1/16)$, the corresponding values of M differ by a factor 4, that results into a gap of about 6 dB.
- *Radar Robustness to Encoding Choices.* Fig. 7 shows that, even under simultaneous illumination, the choice

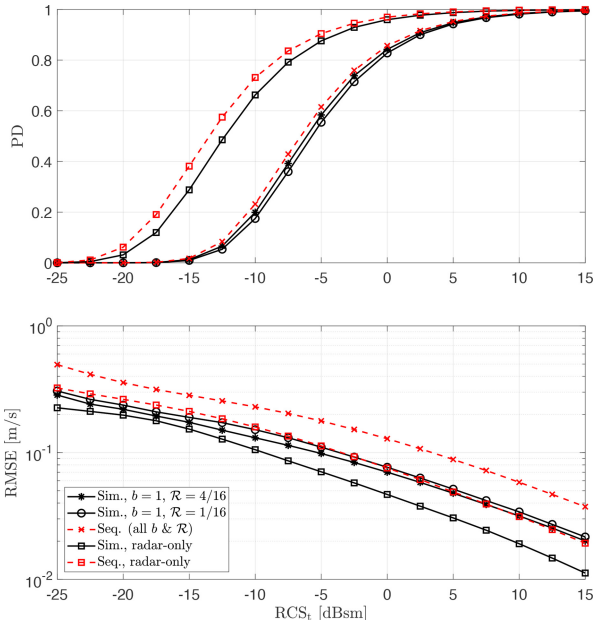

FIGURE 7. PD (top) and RMSE (bottom) versus RCS$_t$ for simultaneous and sequential illumination and for different $(b, \mathcal{R})$ pairs when $\zeta_u = -5$ dB and $\zeta_c = -60$ dB; for comparison, the radar-only scenario (where $\zeta_u = -\infty$ dB) is also included.

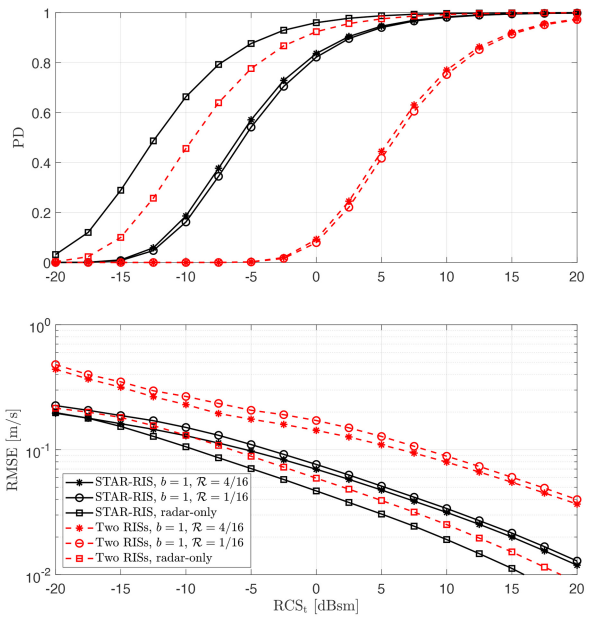

FIGURE 8. PD (top) and RMSE (bottom) versus RCS$_t$ for simultaneous illumination and for two $(b, \mathcal{R})$ pairs when $\zeta_u = -5$ dB and $\zeta_c = -60$ dB; the radar-only case is also considered, and the Two RISs traditional system is included for comparison.

of $(b, \mathcal{R})$ has a negligible impact on radar performance. This further confirms the robustness of the radar function with respect to the specific encoding configuration.

- *Simultaneous vs Sequential Illumination.* For a fixed $(b, \mathcal{R})$, sequential illumination offers several advantages over its simultaneous counterpart. First, it allows halving the time slot duration, which is beneficial when the coherence time of the user channel is limited. Second, it avoids temporal overlap of echoes from the two half-spaces, simplifying implementation of the radar detector as discussed in Section III-C. Third, as illustrated in Fig. 7 (top), it offers slightly improved detection performance. However, this comes at the cost of halving the illumination time per half-space, which doubles the radar Doppler resolution compared to simultaneous illumination. Consequently, sequential illumination results in a higher RMSE, as shown in Fig. 7 (bottom).
- *Impact of Communication on Radar Performance.* Introducing the communication function degrades sensing performance. Compared to the radar-only scenario (where $\zeta_u = -\infty$), a loss of approximately 5 dBsm is observed. This degradation is primarily due to the STAR-RIS redirecting only a portion of the incident power toward the target, while the embedded message has a negligible effect. This is supported by Fig. 5, where the gain toward the target in both the STAR-RIS and two-way array power patterns reduces by about 5 dB when ζ_u is increased from $-\infty$ to -5 dB.

We also provide a quantitative comparison against a *traditional* RIS baseline that achieves full-space coverage using two panels: one transmissive and one reflective, each with $N_{\text{ris}}/2$ elements. This configuration, referred to as the *Two RISs* scheme, ensures the total aperture equals that of the proposed STAR-RIS. We focus on the simultaneous illumination mode, where both RIS panels are active in every PRI, enabling concurrent dual-side sensing and communication. For fairness, the beampattern constraints are set such that the Two RISs system sends the same power toward the users' directions and receives the same power from the clutter region as the STAR-RIS system. Fig. 8 presents PD and RMSE versus RCS$_t$ for the two compared systems; two pairs of $(b, \mathcal{R})$ are reported, along with the radar-only case. Thanks to the adopted setting for the beampattern design, the users in both the STAR-RIS and Two RISs cases experience the same BER. From Fig. 8, it is seen that the proposed STAR-RIS-based architecture gains about 3 dB over the Two-RISs one, in the radar-only case, and about 12 dB, in the ISAC scenario. The superior performance is due to the higher number of elements. Indeed, although each element of the STAR-RISs scheme splits the incident power between the two sides, the double number of elements grants a higher array gain and a higher number of degrees of freedom for beampattern design. In particular, the latter point becomes quite relevant in the presence of the communication function.

Finally, we examine the sensing-communication tradeoff in greater detail by decreasing ζ_u from -2 dB to -70 dB. Fig. 9 presents the resulting values of PD and RMSE versus BER for RCS$_t = 0, 5, 10$ dBsm and two operating scenarios for the users. The radar performance is marginally affected by the communication function when the desired BER is not lower than 10^{-4} for SNR$_{\text{com}} = 11.5$ dB or $5 \cdot 10^{-3}$ for

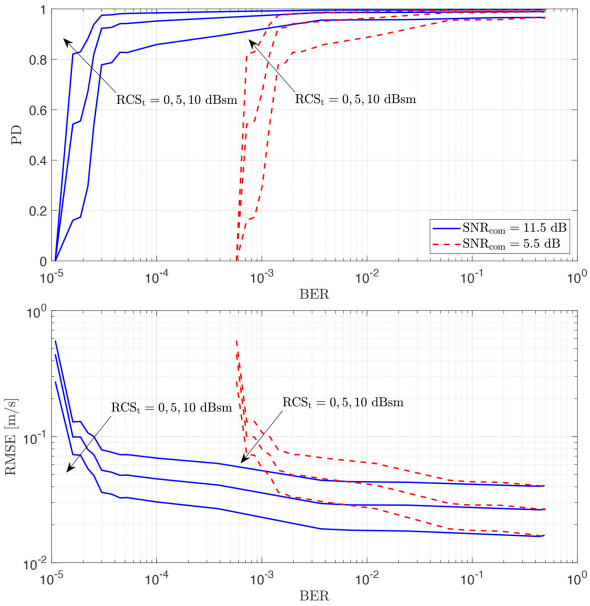

FIGURE 9. PD (top) and RMSE (bottom) versus BER for $\zeta_c = -60$ dB and varying ζ_u, when the simultaneous illumination is adopted, $b = 1$, and $\mathcal{R} = 4/16$. Two operating scenarios are considered for the communication users that correspond to have $\text{SNR}_{\text{com}} = 5.5$ dB and 11.5 dB when $\zeta_u = -5$ dB.

$\text{SNR}_{\text{com}} = 5.5$ dB. Further reducing the BER requires the STAR-RIS to redirect nearly all the incident energy toward the user, which significantly degrades radar performance.

V. CONCLUSION

This paper presented a radar-centric ISAC architecture that exploits a feeder emitting a periodic pulse train, a passive STAR-RIS, and a radar receiver equipped with a PESA and a single digital channel. A joint design of the STAR-RIS spatial response and the radar analog beamformer was proposed to maximize the two-way array power pattern in the directions of interest to the radar, while mitigating clutter and safeguarding communication. Two encoding schemes were introduced to govern the STAR-RIS modulation across pulse repetition intervals, enabling either simultaneous or sequential illumination of the two half-spaces; these schemes support both radar target separability and blind communication decoding through the use of orthogonal binary codewords. Finally, the design of the radar and communication receivers were developed under a GIC-based framework.

The analysis demonstrated that different trade-offs between radar and communication functionalities are achievable by balancing the amounts of power redirected towards prospective targets and users. The proposed encoding schemes also allow for flexible trade-offs between transmission rate and BER with a minimal impact on radar performance, which was evaluated in terms of PD and RMSE in estimating target radial velocity. Notably, simultaneous illumination provides improved velocity estimation due to the processing of a longer pulse train, whereas sequential illumination simplifies radar detection by ensuring non-overlapping echoes from the two half-spaces.

Future work may integrate adaptive or learning-based beamforming strategies to leverage users' CSI and investigate more sophisticated illumination policies for resolving range and/or Doppler ambiguity. Further efforts are also needed to extend the results to more complex and dynamic environments (e.g., correlated multipath or interference), model the impact of hardware impairments, and pursue experimental validation to assess real-world performance.

APPENDIX A
SUBOPTIMUM SOLUTION TO PROBLEM (25)

Let $M_c = \text{card}(\bar{\mathcal{F}}_c)$, $M_u = \text{card}(\bar{\mathcal{F}}_u)$, and $M = M_c + M_u$. Denote by $\{\boldsymbol{\phi}_i\}_{i=1}^{M_c}$ and $\{\boldsymbol{\phi}_i\}_{i=M_c+1}^{M}$ the angular directions contained in the sets $\bar{\mathcal{F}}_c$ and $\bar{\mathcal{F}}_u$, respectively. Let $N = 2N_{\text{ris}} + N_{\text{rad}}$ and define

$$\boldsymbol{s} = \left[\boldsymbol{s}_{\text{tr}}; \boldsymbol{s}_{\text{re}}; \boldsymbol{s}_{\text{rad}}\right] \in \mathbb{C}^N, \tag{42}$$

$$f(\boldsymbol{s}) = -\sum_{\boldsymbol{\phi}\in\bar{\mathcal{F}}_t} \text{A}(\boldsymbol{\phi}; \boldsymbol{s}_{\text{tr}}, \boldsymbol{s}_{\text{re}}, \boldsymbol{s}_{\text{rad}}), \tag{43}$$

$$q_i(\boldsymbol{s}) = \begin{cases} \frac{1}{\zeta_c}\text{A}\left(\boldsymbol{\phi}_i; \boldsymbol{s}_{\text{tr}}, \boldsymbol{s}_{\text{re}}, \boldsymbol{s}_{\text{rad}}\right) - 1, & \text{if } i \le M_c \\ 1 - \frac{1}{\zeta_u}\text{A}_{\text{ris}}\left(\boldsymbol{\phi}_i; \boldsymbol{s}_{\text{tr}}, \boldsymbol{s}_{\text{re}}\right), & \text{if } i > M_c. \end{cases} \tag{44}$$

Then, Problem (25) can be rewritten as

$$\begin{aligned} \min_{\boldsymbol{s}\in\mathbb{C}^N} \quad & f(\boldsymbol{s}), \\ \text{s.t.} \quad & q_i(\boldsymbol{s}) \le 1, \quad i = 1, \ldots, M, \\ & |s_n| = 1, \quad n = 1, \ldots, N. \end{aligned} \tag{45}$$

Next we derive a suboptimal solution to (45) by resorting to the augmented Lagrangian method with partial elimination of the constraints [45]. After introducing the slack variables $\boldsymbol{z} \in \mathbb{R}^M$, the inequality constraints are converted into equality constrains, and Problem (45) is reformulated as

$$\begin{aligned} \min_{\boldsymbol{s}\in\mathbb{C}^N, \boldsymbol{z}\in\mathbb{R}^M} \quad & f(\boldsymbol{s}), \\ \text{s.t.} \quad & q_i(\boldsymbol{s}) + z_i = 0, \quad i = 1, \ldots, M, \\ & z_i \ge 0, \quad i = 1, \ldots, M, \\ & |s_n| = 1, \quad n = 1, \ldots, N. \end{aligned} \tag{46}$$

The augmented Lagrangian for this problem is

$$\begin{aligned} \bar{\mathcal{L}}_\mu(\boldsymbol{s}, \boldsymbol{z}, \boldsymbol{\lambda}) = & f(\boldsymbol{s}) \\ & + \sum_{i=1}^{M}\left[\lambda_i\left(q_i(\boldsymbol{s}) + z_i\right) + \frac{\mu}{2}\left(q_i(\boldsymbol{s}) + z_i\right)^2\right], \end{aligned} \tag{47}$$

where the constraints $|s_i| = 1$ have not been eliminated by means of a penalty. Instead, they are handled directly in the minimization of the Lagrangian function, i.e.,

$$\begin{aligned} \min_{\boldsymbol{s}\in\mathbb{C}^N, \boldsymbol{z}\in\mathbb{R}^M} \quad & \bar{\mathcal{L}}_\mu(\boldsymbol{s}, \boldsymbol{z}, \boldsymbol{\lambda}), \\ \text{s.t.} \quad & z_i \ge 0, \quad i = 1, \ldots, M, \\ & |s_n| = 1, \quad n = 1, \ldots, N. \end{aligned} \tag{48}$$

For fixed $\boldsymbol{s}$, the minimization over $\boldsymbol{z}$ gives $z_i = (-(\lambda_i/\mu + q_i(\boldsymbol{s})))^+$, where $z^+ = \max\{z, 0\}$. Therefore, the constraint $q_i(\boldsymbol{s}) + z_i = 0$ in (46) becomes $\max\{q_i(\boldsymbol{s}), -\lambda_i/\mu\} = 0$, and Problem (48) reduces to

$$\min_{\boldsymbol{s}\in\mathbb{C}^N} \mathcal{L}_\mu(\boldsymbol{s}, \boldsymbol{\lambda}), \quad \text{s.t. } |s_n| = 1, \quad n = 1, \ldots, N. \tag{49}$$

where

$$\mathcal{L}_\mu(\boldsymbol{s}, \boldsymbol{\lambda}) = f(\boldsymbol{s}) + \frac{1}{2\mu}\sum_{i=1}^{M}\left[\left(\left(\lambda_i + \mu q_i(\boldsymbol{s})\right)^+\right)^2 - \lambda_i^2\right]. \tag{50}$$

Problem (49) can be solved using the gradient projection method; in this case, the n-th iteration takes the form

$$\boldsymbol{s}^{(n)} = \Pi\left(\boldsymbol{s}^{(n-1)} - \xi^{(n)}\nabla\mathcal{L}_\mu\left(\boldsymbol{s}^{(n-1)}, \boldsymbol{\lambda}\right)\right), \tag{51}$$

where Π is the projector on the N-dimensional unit-modulus torus (i.e., $\Pi(\boldsymbol{s}) = \boldsymbol{\omega} \in \mathbb{C}^N$, with $\omega_i = s_i/|s_i|$, for $i = 1, \ldots, N$), $\xi^{(n)}$ is the stepsize at the n-th iteration, and

$$\nabla\mathcal{L}_\mu(\boldsymbol{s}, \boldsymbol{\lambda}) = \nabla f(\boldsymbol{s}) + \sum_{i=1}^{M}\left(\lambda_i + \mu q_i(\boldsymbol{s})\right)^+\nabla q_i(\boldsymbol{s}), \tag{52}$$

is the gradient of $L_\mu(\boldsymbol{s}, \boldsymbol{\lambda})$. From (19), (43), and (44),

$$\nabla f(\boldsymbol{s}) = -\sum_{\boldsymbol{\phi}\in\bar{\mathcal{F}}_{\rm t}}\begin{bmatrix}\frac{\partial \mathrm{A}_{\rm ris}(\boldsymbol{\phi};\boldsymbol{s}_{\rm tr},\boldsymbol{s}_{\rm re})}{\partial \boldsymbol{s}_{\rm tr}}\mathrm{A}_{\rm rad}(\boldsymbol{\phi};\boldsymbol{s}_{\rm rad})\\ \frac{\partial \mathrm{A}_{\rm ris}(\boldsymbol{\phi};\boldsymbol{s}_{\rm tr},\boldsymbol{s}_{\rm re})}{\partial \boldsymbol{s}_{\rm re}}\mathrm{A}_{\rm rad}(\boldsymbol{\phi};\boldsymbol{s}_{\rm rad})\\ \mathrm{A}_{\rm ris}(\boldsymbol{\phi};\boldsymbol{s}_{\rm tr},\boldsymbol{s}_{\rm re})\frac{\partial \mathrm{A}_{\rm rad}(\boldsymbol{\phi};\boldsymbol{s}_{\rm rad})}{\partial \boldsymbol{s}_{\rm tr}}\end{bmatrix}, \tag{53a}$$

$$\nabla q_i(\boldsymbol{s}) = \begin{cases}\frac{1}{\zeta_c}\begin{bmatrix}\frac{\partial \mathrm{A}_{\rm ris}(\boldsymbol{\phi}_i;\boldsymbol{s}_{\rm tr},\boldsymbol{s}_{\rm re})}{\partial \boldsymbol{s}_{\rm tr}}\mathrm{A}_{\rm rad}(\boldsymbol{\phi}_i;\boldsymbol{s}_{\rm rad})\\ \frac{\partial \mathrm{A}_{\rm ris}(\boldsymbol{\phi}_i;\boldsymbol{s}_{\rm tr},\boldsymbol{s}_{\rm re})}{\partial \boldsymbol{s}_{\rm re}}\mathrm{A}_{\rm rad}(\boldsymbol{\phi}_i;\boldsymbol{s}_{\rm rad})\\ \mathrm{A}_{\rm ris}(\boldsymbol{\phi}_i;\boldsymbol{s}_{\rm tr},\boldsymbol{s}_{\rm re})\frac{\partial \mathrm{A}_{\rm rad}(\boldsymbol{\phi}_i;\boldsymbol{s}_{\rm rad})}{\partial \boldsymbol{s}_{\rm tr}}\end{bmatrix}, & \text{if } i \le M_{\rm c},\\ -\frac{1}{\zeta_u}\begin{bmatrix}\frac{\partial \mathrm{A}_{\rm ris}(\boldsymbol{\phi}_i;\boldsymbol{s}_{\rm tr},\boldsymbol{s}_{\rm re})}{\partial \boldsymbol{s}_{\rm tr}}\\ \frac{\partial \mathrm{A}_{\rm ris}(\boldsymbol{\phi}_i;\boldsymbol{s}_{\rm tr},\boldsymbol{s}_{\rm re})}{\partial \boldsymbol{s}_{\rm re}}\\ \mathbf{0}_{N_{\rm rad}}\end{bmatrix}, & \text{if } i \ge M_{\rm c}+1,\end{cases} \tag{53b}$$

where, from (6), (7a), (7b), and (9),

$$\frac{\partial \mathrm{A}_{\rm ris}(\boldsymbol{\phi};\boldsymbol{s}_{\rm tr},\boldsymbol{s}_{\rm re})}{\partial \boldsymbol{s}_{\rm tr}} = \frac{2}{\|\boldsymbol{g}\|_1^2}\left(\boldsymbol{u}_{\rm ris}^{\mathsf{T}}(\boldsymbol{\phi})\mathrm{diag}\{\boldsymbol{g}\}\boldsymbol{s}_{\rm tr}\right) \times \mathrm{diag}\{\boldsymbol{g}^*\}\boldsymbol{u}_{\rm ris}^*(\boldsymbol{\phi})\mathbb{1}_{\{\boldsymbol{\phi}\in\mathcal{F}_{\rm tr}\}}, \tag{54a}$$

$$\frac{\partial \mathrm{A}_{\rm ris}(\boldsymbol{\phi};\boldsymbol{s}_{\rm tr},\boldsymbol{s}_{\rm re})}{\partial \boldsymbol{s}_{\rm re}} = \frac{2}{\|\boldsymbol{g}\|_1^2}\left(\boldsymbol{u}_{\rm ris}^{\mathsf{T}}(\boldsymbol{\phi})\mathrm{diag}\{\boldsymbol{g}\}\boldsymbol{s}_{\rm re}\right) \times \mathrm{diag}\{\boldsymbol{g}^*\}\boldsymbol{u}_{\rm ris}^*(\boldsymbol{\phi})\mathbb{1}_{\{\boldsymbol{\phi}\in\mathcal{F}_{\rm tr}\}}, \tag{54b}$$

$$\frac{\partial \mathrm{A}_{\rm rad}(\boldsymbol{\phi};\boldsymbol{s}_{\rm rad})}{\partial \boldsymbol{s}_{\rm rad}} = \frac{2}{N_{\rm rad}^2}\left(\boldsymbol{u}_{\rm rad}^{\mathsf{H}}(\boldsymbol{\phi})\boldsymbol{s}_{\rm rad}\right)\boldsymbol{u}_{\rm rad}(\boldsymbol{\phi}). \tag{54c}$$

In summary, the augmented Lagrangian method proceeds as follows [46]. Given the multipliers $\boldsymbol{\lambda}^{(k)}$ and the penalty $\mu^{(k)}$ at epoch k, Problem (49) is approximately solved, thereby obtaining $\boldsymbol{s}^{(k)}$. Then, the multipliers are updated as

$$\lambda_i^{(k+1)} = \left(\lambda_i^{(k)} + \mu^{(k)}q_i\left(\boldsymbol{s}^{(k)}\right)\right)^+, \quad i = 1, \ldots, M, \tag{55}$$

a new penalty parameter $\mu^{(k+1)} \ge \mu^{(k)}$ is chosen, and the process is repeated. Alg. 1 summarizes the procedure.

Algorithm 1 Sub-Optimal Solution to Problem (45)

choose $\boldsymbol{s} \in \mathbb{C}^N$, $\boldsymbol{\lambda} \in \mathbb{R}^M$, $\eta^\star \in \mathbb{R}$, and $\omega^\star \in \mathbb{R}$
Set $\mu = 10$, $\omega = 0.1$, and $\eta = 0.1$
repeat
  $\omega = \max\{\omega^\star, \omega/2^{0.5}\}$
  repeat
    compute $\nabla\mathcal{L}_\mu(\boldsymbol{s}, \boldsymbol{\lambda})$
    set the stepsize ξ
    $\boldsymbol{s} = \Pi\left(\boldsymbol{s} - \xi\nabla\mathcal{L}_\mu(\boldsymbol{s}, \boldsymbol{\lambda})\right)$
  until $\|\boldsymbol{s} - \Pi\left(\boldsymbol{s} - \xi\nabla\mathcal{L}_\mu(\boldsymbol{s}, \boldsymbol{\lambda})\right)\|_\infty \le \omega$
  if $\max_{i=1,\ldots,M}\left|\max\left\{q_i(\boldsymbol{s}), -\lambda_i/\mu\right\}\right| \le \eta$ **then**
    $\lambda_i = \left(\lambda_i + \mu q_i(\boldsymbol{s})\right)^+$, for $i = 1, \ldots, M$,
    $\eta = \max\{\eta^\star, \eta/(1 + \mu^{0.5})\}$
  else
    $\mu = 10\mu$
    $\eta = \max\{\eta^\star, 0.1/(1 + \mu^{0.1})\}$
  end if
until $\max_{i=1,\ldots,M}\max\left|\left\{g_i(\boldsymbol{s}), -\lambda_i/\mu\right\}\right| \le \eta^\star$ and $\|\boldsymbol{s} - \xi\Pi\left(\boldsymbol{s} - \nabla\mathcal{L}_\mu(\boldsymbol{s}, \boldsymbol{\lambda})\right)\|_\infty \le \omega^\star$
return $\boldsymbol{s}$

APPENDIX B
DERIVATION OF THE DECODING RULE IN (36)

Let $\boldsymbol{\beta} \in \mathbb{C}^J$, with $J \in \mathcal{J} = \{1, \ldots, L_{{\rm tr},u}\}$ be the vector containing the non-zero entries of the channel taps $\{\beta_{{\rm tr},u}(\ell)\}_{\ell=0}^{L_{{\rm tr},u}-1}$, and $\{d_j\}_{j=1}^J$ be the corresponding indexes, whereby $\beta_{{\rm tr},u}(d_j - 1) = \beta_j$, for $j = 1, \ldots, J$. Then, the samples in Eq. (24a) can be organized in the matrix $\boldsymbol{Y} \in \mathbb{C}^{M\times J}$, with $[\boldsymbol{Y}]_{p,\ell} = y_{{\rm tr},u}(p-1, \ell-1)$, and

$$\boldsymbol{Y} = \boldsymbol{c}\sum_{j=1}^{J}\beta_j\boldsymbol{e}_{d_j}^{\mathsf{T}} + \boldsymbol{Z}, \tag{56}$$

where $\boldsymbol{c} = [c_{{\rm tr},u}(0) \cdots c_{{\rm tr},u}(M-1)]^{\mathsf{T}} \in \mathcal{C}_{\rm tr}$ is the codeword sent in $[0, MT]$, $\boldsymbol{e}_i \in \mathbb{R}^J$ is a vector whose entries are all zero, except the i-th one that equals 1, and $\boldsymbol{Z} \in \mathbb{C}^{M\times J}$ is the noise matrix, with $[\boldsymbol{Z}]_{p,\ell} = z_{{\rm tr},u}(p-1, \ell-1)$.

The user is faced with the problem of estimating $\boldsymbol{c}$ based on $\boldsymbol{Y}$, when J and $\{(\beta_j, d_j)\}_{j=1}^J$ are unknown, and the entries of $\boldsymbol{Z}$ are i.i.d. complex circularly-symmetric Gaussian random variables with variance $\sigma_{\rm com}^2$. Next, we use the GIC rule to estimate the number of non-zero channel taps [42]. To proceed, write the log-likelihood under the hypothesis that J entries are non-zero, namely

$$\mathcal{L}_J\left(\boldsymbol{Y}; \boldsymbol{c}, \{\beta_j\}_{j=1}^J, \{d_j\}_{j=1}^J\right) = -\frac{1}{\sigma_{\rm com}^2}\left\|\boldsymbol{Y} - \boldsymbol{c}\sum_{j=1}^{J}\beta_j\boldsymbol{e}_{d_j}^{\mathsf{T}}\right\|_F^2 - MJ\ln\left(\pi\sigma_{\rm com}^2\right). \tag{57}$$

Under this hypothesis, the ML estimators of the codeword and of the tap amplitudes and indexes, $\hat{\boldsymbol{c}}$ and $\{(\hat{\beta}_j, \hat{d}_j)\}_{j=1}^J$,

respectively, are found by solving

$$\max_{\substack{\boldsymbol{c}\in\mathcal{C}_{\rm tr},\{\beta_j\}_{j=1}^J\in\mathbb{C},\\ \{d_j\}_{j=1}^J\in\mathcal{J}}} \mathcal{L}_J\Big(\boldsymbol{Y};\boldsymbol{c},\{\beta_j\}_{j=1}^J,\{d_j\}_{j=1}^J\Big). \tag{58}$$

Then, the number of non-zero entries, say $\hat{J}$, is obtained with a GIC rule, i.e., by solving

$$\min_{J\in\mathcal{J}}\Big\{J\eta'_{\rm com}-\mathcal{L}_J\Big(\boldsymbol{Y};\hat{\boldsymbol{c}},\{\hat{\beta}_j\}_{j=1}^J,\{\hat{d}_j\}_{j=1}^J\Big)\Big\}, \tag{59}$$

where $\eta'_{\rm com}$ is a penalty factor. Finally, the codeword is decoded by taking the ML estimator $\hat{\boldsymbol{c}}$ when $J=\hat{J}$.

Combining (58) and (59), the GIC rule is

$$\min_{J\in\mathcal{J}}\Bigg\{\ J\eta'_{\rm com} - \max_{\substack{\boldsymbol{c}\in\mathcal{C}_{\rm tr},\{\beta_j\}_{j=1}^J\in\mathbb{C},\\ \{d_j\}_{j=1}^J\in\mathcal{J}}} \mathcal{L}_J\Big(\boldsymbol{Y};\boldsymbol{c},\{\beta_j\}_{j=1}^J,\{d_j\}_{j=1}^J\Big)\Bigg\}, \tag{60}$$

which is equivalent to

$$\max_{J\in\mathcal{J}}\max_{\substack{\boldsymbol{c}\in\mathcal{C}_{\rm tr},\{\beta_j\}_{j=1}^J\in\mathbb{C},\\ \{d_j\}_{j=1}^J\in\mathcal{J}}}\Big\{\mathcal{L}_J\Big(\boldsymbol{Y};\boldsymbol{c},\{\beta_j\}_{j=1}^J,\{d_j\}_{j=1}^J\Big) - J\eta'_{\rm com}\Big\}. \tag{61}$$

Since the maximization in (58) is equivalent to the inner maximization in (61), the optimum $\boldsymbol{c}$ obtained by solving (61) is also equal to the ML estimator $\hat{\boldsymbol{c}}$ when $J=\hat{J}$, i.e., to the decoded codeword. We, therefore, proceed by solving Problem (61). Upon denoting $\eta_{\rm com}=\sigma^2_{\rm com}\eta'_{\rm com}$, Problem (61) is equivalent to

$$\max_{\boldsymbol{c}\in\mathcal{C}_{\rm tr}}\max_{J\in\mathcal{J}}\max_{\substack{\{\beta_j\}_{j=1}^J\in\mathbb{C},\\ \{d_j\}_{j=1}^J\in\mathcal{J}}}\Big\{-\Big\|\boldsymbol{Y}-\boldsymbol{c}\sum_{j=1}^J\beta_j\boldsymbol{e}_{d_j}^{\mathsf{T}}\Big\|_F^2-J\eta_{\rm com}\Big\}. \tag{62}$$

Let us start by tackling the minimization over $\{\beta_j\}_{j=1}^J$, and let $\boldsymbol{A}_j=\boldsymbol{c}\boldsymbol{e}_{d_j}^{\mathsf{T}}$, $j=1,\ldots,J$. Then, conditions for the minimum over $\{\beta_j\}_{j=1}^J$ are

$$\begin{aligned}0&=\frac{\partial}{\partial\beta_j}\Big\{-\Big\|\boldsymbol{Y}-\sum_{i=1,\,i\neq j}^J\alpha_i\boldsymbol{A}_i-\beta_j\boldsymbol{A}_j\Big\|_F^2-J\eta_{\rm com}\Big\}\\ &=2{\rm Tr}\Big(\Big(\boldsymbol{Y}-\sum_{i=1,\,i\neq j}^J\alpha_i\boldsymbol{A}_i\Big)\boldsymbol{A}_j^{\mathsf{H}}\Big)-2\beta_j{\rm Tr}\Big(\boldsymbol{A}_j\boldsymbol{A}_j^{\mathsf{H}}\Big)\\ &=2\boldsymbol{c}^{\mathsf{H}}\boldsymbol{Y}\boldsymbol{e}_{d_j}-2\|\boldsymbol{c}\|^2\beta_j,\quad j=1,\ldots,J,\end{aligned} \tag{63}$$

where the last equality follows from the fact that ${\rm Tr}(\boldsymbol{A}_i\boldsymbol{A}_j^{\mathsf{H}})=\|\boldsymbol{c}\|^2$, if $i=j$, and zero, otherwise. Therefore

$$\beta_j=\frac{\boldsymbol{c}^{\mathsf{H}}\boldsymbol{Y}\boldsymbol{e}_{d_j}}{\|\boldsymbol{c}\|^2},\quad j=1,\ldots,J, \tag{64}$$

and Problem (62) becomes

$$\max_{\boldsymbol{c}\in\mathcal{C}_{\rm tr}}\max_{J\in\mathcal{J}}\max_{\{d_j\}_{j=1}^J\in\mathcal{J}}\Big\{-\Big\|\boldsymbol{Y}-\frac{\boldsymbol{c}\boldsymbol{c}^{\mathsf{H}}}{\|\boldsymbol{c}\|^2}\boldsymbol{Y}\sum_{j=1}^J\boldsymbol{e}_{d_j}\boldsymbol{e}_{d_j}^{\mathsf{T}}\Big\|_F^2 \tag{65}$$

$$-J\eta_{\rm com}\Big\}. \tag{66}$$

Notice now that $\boldsymbol{E}=\sum_{j=1}^J\boldsymbol{e}_{d_j}\boldsymbol{e}_{d_j}\in\mathbb{R}^{J\times J}$ appearing in (66) is a square matrix whose entries are all zero, except those in positions $\{(d_j,d_j)\}_{j=1}^J$ that equals 1. Then, the Frobenius norm in (66) can also be written as

$$\begin{aligned}\Big\|\boldsymbol{Y}-\frac{\boldsymbol{c}\boldsymbol{c}^{\mathsf{H}}}{\|\boldsymbol{c}\|^2}\boldsymbol{Y}\boldsymbol{E}\Big\|_F^2&={\rm Tr}\Big(\boldsymbol{Y}\boldsymbol{Y}^{\mathsf{H}}\Big)\\ &\quad-\frac{2}{\|\boldsymbol{c}\|^2}\Re\Big({\rm Tr}\Big(\boldsymbol{Y}\boldsymbol{E}\boldsymbol{Y}^{\mathsf{H}}\boldsymbol{c}\boldsymbol{c}^{\mathsf{H}}\Big)\Big)\\ &\quad+\frac{1}{\|\boldsymbol{c}\|^4}{\rm Tr}\Big(\boldsymbol{c}\boldsymbol{c}^{\mathsf{H}}\boldsymbol{Y}\boldsymbol{E}\boldsymbol{E}\boldsymbol{Y}^{\mathsf{H}}\boldsymbol{c}\boldsymbol{c}^{\mathsf{H}}\Big)\\ &={\rm Tr}\Big(\boldsymbol{Y}\boldsymbol{Y}^{\mathsf{H}}\Big)-\frac{\boldsymbol{c}^{\mathsf{H}}\boldsymbol{Y}\boldsymbol{E}\boldsymbol{Y}^{\mathsf{H}}\boldsymbol{c}}{\|\boldsymbol{c}\|^2}\\ &={\rm Tr}\Big(\boldsymbol{Y}\boldsymbol{Y}^{\mathsf{H}}\Big)-\frac{\|\boldsymbol{c}^{\mathsf{H}}\boldsymbol{Y}\boldsymbol{E}\|^2}{\|\boldsymbol{c}\|^2}\\ &={\rm Tr}\Big(\boldsymbol{Y}\boldsymbol{Y}^{\mathsf{H}}\Big)-\sum_{\ell\in\{d_j\}_{j=1}^J}\frac{\big|\big(\boldsymbol{c}^{\mathsf{H}}\boldsymbol{Y}\big)_\ell\big|^2}{\|\boldsymbol{c}\|^2}\\ &={\rm Tr}\Big(\boldsymbol{Y}\boldsymbol{Y}^{\mathsf{H}}\Big)-\sum_{\ell\in\{d_j\}_{j=1}^J}T_{\rm tr}(\boldsymbol{c},\ell-1),\end{aligned} \tag{67}$$

whereby Problem (66) is equivalent to

$$\max_{\boldsymbol{c}\in\mathcal{C}_{\rm tr}}\max_{J\in\mathcal{J}}\max_{\{d_j\}_{j=1}^J\in\mathcal{J}}\Big\{\sum_{\ell\in\{d_j\}_{j=1}^J}T_{\rm tr}(\boldsymbol{c},\ell-1)-J\eta_{\rm com}\Big\}. \tag{68}$$

The maximization over $\{d_j\}_{j=1}^J$ amounts to taking the J indexes with largest statistic. If we compute the order statistics $\{T_{\rm tr}^{\rm sort}(\boldsymbol{c},\ell)\}_{\ell=0}^{L_{{\rm tr},u}-1}$ by sorting $\{T_{\rm tr}(\boldsymbol{c},\ell)\}_{\ell=0}^{L_{{\rm tr},u}-1}$ in decreasing order, Problem (68) reduces to

$$\begin{aligned}&\max_{\boldsymbol{c}\in\mathcal{C}_{\rm tr}}\max_{J\in\mathcal{J}}\Big\{\Big\{\sum_{\ell=0}^{J-1}T_{\rm tr}^{\rm sort}(\boldsymbol{c},\ell)-J\eta_{\rm com}\Big\}\\ &\quad=\max_{\boldsymbol{c}\in\mathcal{C}_{\rm tr}}\Big\{T_{\rm tr}^{\rm sort}(\boldsymbol{c},0)-\eta_{\rm com}\\ &\qquad+\sum_{\ell=1}^{L_{{\rm tr},u}-1}\big(T_{\rm tr}^{\rm sort}(\boldsymbol{c},\ell)-\eta_{\rm com}\big)^+\Big\}.\end{aligned} \tag{69}$$

which is equivalent to (36).

REFERENCES

[1] O. Tsilipakos et al., "Toward intelligent metasurfaces: The progress from globally tunable metasurfaces to software-defined metasurfaces with an embedded network of controllers," *Adv. Opt. Mater.*, vol. 8, no. 17, 2020, Art. no. 2000783.

[2] Q. Wu, S. Zhang, B. Zheng, C. You, and R. Zhang, "Intelligent reflecting surface-aided wireless communications: A tutorial," *IEEE Trans. Commun.*, vol. 69, no. 5, pp. 3313–3351, May 2021.

[3] Y. Liu et al., "Reconfigurable intelligent surfaces: Principles and opportunities," *IEEE Commun. Surveys Tuts.*, vol. 23, no. 3, pp. 1546–1577, 3rd Quart., 2021.

[4] C. Pan et al., "Reconfigurable intelligent surfaces for 6G systems: Principles, applications, and research directions," *IEEE Wireless Commun. Mag.*, vol. 59, no. 6, pp. 14–20, Jun. 2021.

[5] E. Björnson, H. Wymeersch, B. Matthiesen, P. Popovski, L. Sanguinetti, and E. de Carvalho, "Reconfigurable intelligent surfaces: A signal processing perspective with wireless applications," *IEEE Signal Process. Mag.*, vol. 39, no. 2, pp. 135–158, Mar. 2022.

[6] L. Zhang et al., "Space-time-coding digital metasurfaces," *Nat. Commun.*, vol. 9, p. 4334, Oct. 2018.

[7] V. Jamali, A. M. Tulino, G. Fischer, R. R. Müller, and R. Schober, "Intelligent surface-aided transmitter architectures for millimeter-wave ultra massive MIMO systems," *IEEE Open J. Commun. Soc.*, vol. 2, pp. 144–167, 2021.

[8] Q. Li, M. Wen, and M. Di Renzo, "Single-RF MIMO: From spatial modulation to metasurface-based modulation," *IEEE Wireless Commun.*, vol. 28, no. 4, pp. 88–95, Aug. 2021.

[9] C. D'Elia, E. Grossi, and L. Venturino, "Beampattern design for transmit architectures based on reconfigurable intelligent surfaces," *IEEE Trans. Veh. Technol.*, early access, Jul. 10, 2025, doi: 10.1109/TVT.2025.3588263.

[10] L. Zhang, M. Rossi, X. Q. Chen, G. Castaldi, T. J. Cui, and V. Galdi, "Some emerging concepts in the design of space-time-coding digital metasurfaces," in *Proc. 18th Int. Congr. Artif. Mater. Novel Wave Phenomena (Metamaterials)*, 2024, pp. 1–3.

[11] M. Mizmizi, D. Tagliaferri, and U. Spagnolini, "Wireless communications with space–time modulated metasurfaces," *IEEE J. Sel. Areas Commun.*, vol. 42, no. 6, pp. 1534–1548, Jun. 2024.

[12] M. Di Renzo et al., "Smart radio environments empowered by reconfigurable intelligent surfaces: How it works, state of research, and the road ahead," *IEEE J. Sel. Areas Commun.*, vol. 38, no. 11, pp. 2450–2525, Nov. 2020.

[13] Q. Wu and R. Zhang, "Towards smart and reconfigurable environment: Intelligent reflecting surface aided wireless network," *IEEE Commun. Mag.*, vol. 58, no. 1, pp. 106–112, Jan. 2020.

[14] K. Zhi, C. Pan, H. Ren, K. K. Chai, and M. Elkashlan, "Active RIS versus passive RIS: Which is superior with the same power budget?" *IEEE Wireless Commun. Lett.*, vol. 26, no. 5, pp. 1150–1154, May 2022.

[15] Z. Zhang et al., "Active RIS vs. passive RIS: Which will prevail in 6G?" *IEEE Trans. Commun.*, vol. 71, no. 3, pp. 1707–1725, Mar. 2023.

[16] E. Grossi, H. Taremizadeh, and L. Venturino, "Radar target detection and localization aided by an active reconfigurable intelligent surface," *IEEE Signal Process. Lett.*, vol. 30, pp. 903–907, 2023.

[17] P. Saikia, A. Jee, K. Singh, W.-J. Huang, A.-A. A. Boulogeorgos, and T. A. Tsiftsis, "Hybrid-RIS empowered UAV-assisted ISAC systems: Transfer learning-based DRL," *IEEE Trans. Commun.*, vol. 73, no. 9, pp. 8314–8329, Sep. 2025.

[18] J. Xu, Y. Liu, X. Mu, and O. A. Dobre, "STAR-RISs: Simultaneous transmitting and reflecting reconfigurable intelligent surfaces," *IEEE Wireless Commun. Lett.*, vol. 25, no. 9, pp. 3134–3138, Sep. 2021.

[19] X. Mu, Y. Liu, L. Guo, J. Lin, and R. Schober, "Simultaneously transmitting and reflecting (STAR) RIS aided wireless communications," *IEEE Trans. Wireless Commun.*, vol. 21, no. 5, pp. 3083–3098, May 2022.

[20] J. Xu, Y. Liu, X. Mu, R. Schober, and H. V. Poor, "STAR-RISs: A correlated T&R phase-shift model and practical phase-shift configuration strategies," *IEEE J. Sel. Topics Signal Process.*, vol. 16, no. 5, pp. 1097–1111, Aug. 2022.

[21] M. Ahmed et al., "A survey on STAR-RIS: Use cases, recent advances, and future research challenges," *IEEE Internet Things J.*, vol. 10, no. 16, pp. 14689–14711, Aug. 2023.

[22] J. Xu et al., "Simultaneously transmitting and reflecting intelligent omni-surfaces: Modeling and implementation," *IEEE Veh. Technol. Mag.*, vol. 17, no. 2, pp. 46–54, Jun. 2022.

[23] Q. Li, M. El-Hajjar, Y. Sun, I. Hemadeh, A. Shojaeifard, and L. Hanzo, "Energy-efficient reconfigurable holographic surfaces operating in the presence of realistic hardware impairments," *IEEE Trans. Commun.*, vol. 72, no. 8, pp. 5226–5238, Aug. 2024.

[24] Q. Li, M. El-Hajjar, Y. Sun, and L. Hanzo, "Performance analysis of reconfigurable holographic surfaces in the near-field scenario of cell-free networks under hardware impairments," *IEEE Trans. Wireless Commun.*, vol. 23, no. 9, pp. 11972–11984, Sep. 2024.

[25] Q. Li, M. El-Hajjar, C. Xu, J. An, C. Yuen, and L. Hanzo, "Stacked intelligent metasurfaces for holographic MIMO-aided cell-free networks," *IEEE Trans. Commun.*, vol. 72, no. 11, pp. 7139–7151, Nov. 2024.

[26] Q. Li, M. El-Hajjar, K. Cao, C. Xu, H. Haas, and L. Hanzo, "Holographic metasurface-based beamforming for multi-altitude LEO satellite networks," *IEEE Trans. Wireless Commun.*, vol. 24, no. 4, pp. 3103–3116, Apr. 2025.

[27] D. K. Pin Tan et al., "Integrated sensing and communication in 6G: Motivations, use cases, requirements, challenges and future directions," in *Proc. 1st IEEE Int. Online Symp. Joint Commun. Sens. (JC&S)*, 2021, pp. 1–6.

[28] Y. Cui, F. Liu, X. Jing, and J. Mu, "Integrating sensing and communications for ubiquitous IoT: Applications, trends, and challenges," *IEEE Netw.*, vol. 35, no. 5, pp. 158–167, Sep./Oct. 2021.

[29] J. A. Zhang et al., "Enabling joint communication and radar sensing in mobile networks—A survey," *IEEE Commun. Surveys Tuts.*, vol. 24, no. 1, pp. 306–345, 1st Quart., 2022.

[30] F. Liu et al., "Integrated sensing and communications: Toward dual-functional wireless networks for 6G and beyond," *IEEE J. Sel. Areas Commun.*, vol. 40, no. 6, pp. 1728–1767, Jun. 2022.

[31] A. Magbool, V. Kumar, Q. Wu, M. Di Renzo, and M. F. Flanagan, "A survey on integrated sensing and communication with intelligent metasurfaces: Trends, challenges, and opportunities," *IEEE Open J. Commun. Soc.*, vol. 6, pp. 7270–7318, 2025.

[32] S. Zhang, W. Hao, G. Sun, Z. Zhu, X. Li, and Q. Wu, "Joint beamforming design for the STAR-RIS-enabled ISAC systems with multiple targets and multiple users," *IEEE Trans. Commun.*, vol. 73, no. 1, pp. 693–708, Jan. 2025.

[33] Z. Liu, X. Li, H. Ji, H. Zhang, and V. C. M. Leung, "Exploiting STAR-RIS for covert communication in ISAC networks under imperfect CSI," *IEEE Trans. Veh. Technol.*, vol. 74, no. 1, pp. 786–802, Jan. 2025.

[34] Y. Wang et al., "Optimizing the fairness of STAR-RIS and NOMA assisted integrated sensing and communication systems," *IEEE Trans. Wireless Commun.*, vol. 23, no. 6, pp. 5895–5907, Jun. 2024.

[35] Z. Zhang, Y. Liu, Z. Wang, and J. Chen, "STARS-ISAC: How many sensors do we need?" *IEEE Trans. Wireless Commun.*, vol. 23, no. 2, pp. 1085–1099, Feb. 2024.

[36] Z. Wang, X. Mu, and Y. Liu, "STARS enabled integrated sensing and communications," *IEEE Trans. Wireless Commun.*, vol. 22, no. 10, pp. 6750–6765, Oct. 2023.

[37] P. Saikia, A. Jee, K. Singh, C. Pan, W.-J. Huang, and T. A. Tsiftsis, "RIS-Aided integrated sensing and communication systems: STAR-RIS versus passive RIS?" *IEEE Open J. Commun. Soc.*, vol. 5, pp. 7954–7973, 2024.

[38] J. Zhang et al., "Intelligent waveform design for integrated sensing and communication," *IEEE Wireless Commun.*, vol. 32, no. 1, pp. 166–173, Feb. 2025.

[39] Z. Yigit and E. Basar, "Hybrid STAR-RIS enabled integrated sensing and communication," *IEEE Trans. Commun.*, vol. 73, no. 9, pp. 8289–8300, Sep. 2025.

[40] E. Grossi, H. Taremizadeh, and L. Venturino, "STAR-RIS-based pulse-doppler radars," in *Proc. 32nd Eur. Signal Process. Conf.*, Lyon, France, Aug. 2024, pp. 2427–2431.

[41] H. Taremizadeh, E. Grossi, and L. Venturino, "STAR-RIS transceivers: Integrated sensing and communication with pulsed signals," in *Proc. 33rd Eur. Signal Process. Conf.*, Sep. 2025, pp. 1–5.

[42] P. Stoica and Y. Selen, "Model-order selection: A review of information criterion rules," *IEEE Signal Process. Mag.*, vol. 21, no. 4, pp. 36–47, Jul. 2004.

[43] H. L. Van Trees, *Detection, Estimation, and Modulation Theory, Part IV: Optimum Array Processing*. New York, NY, USA: Wiley, 2002.

[44] G. C. Alexandropoulos, N. Shlezinger, I. Alamzadeh, M. F. Imani, H. Zhang, and Y. C. Eldar, "Hybrid reconfigurable intelligent metasurfaces: Enabling simultaneous tunable reflections and sensing for 6G wireless communications," *IEEE Veh. Technol. Mag.*, vol. 19, no. 1, pp. 75–84, Mar. 2024.

[45] D. P. Bertsekas, *Constrained Optimization and Lagrange Multiplier Methods*. Belmont, MA, USA: Athena Scientific, 1996.

[46] J. Nocedal and S. Wright, *Numerical Optimization*, 2nd ed. New York, NY, USA: Springer, 2006.
[47] L. Venturino, E. Grossi, M. Lops, J. Johnston, and X. Wang, "Radar-enabled ambient backscatter communications," *IEEE Trans. Wireless Commun.*, vol. 22, no. 12, pp. 8666–8680, Dec. 2023.
[48] E. Grossi, M. Lops, A. M. Tulino, and L. Venturino, "Opportunistic sensing using mmWave communication signals: A subspace approach," *IEEE Trans. Wireless Commun.*, vol. 20, no. 7, pp. 4420–4434, Jul. 2021.
[49] Y. Lai, L. Venturino, E. Grossi, and W. Yi, "Joint detection and localization in distributed MIMO radars employing waveforms with imperfect auto- and cross-correlation," *IEEE Trans. Veh. Technol.*, vol. 72, no. 12, pp. 16524–16537, Dec. 2023.
[50] M. A. Richards, *Fundamentals of Radar Signal Processing*, 2nd ed. New York, NY, USA: McGraw-Hill, 2005.

HEDIEH TAREMIZADEH received the M.Sc. degree in telecommunications engineering from the University of Cassino and Southern Lazio, Italy, in 2022, where she is currently pursuing the Ph.D. degree. Her research interests include reconfigurable intelligent surfaces, radar sensing, and integrated sensing and communications.

EMANUELE GROSSI (Senior Member, IEEE) received the Dr.Eng. degree in telecommunications engineering and the Ph.D. degree in electrical engineering from the University of Cassino and Southern Lazio, Italy, in 2002 and 2006, respectively, where he is an Associate Professor with the Department of Electrical and Information Engineering. In 2005, he was a Visiting Scholar with the Department of Electrical and Computer Engineering, University of British Columbia, Canada, and held a visiting appointment with the Digital Technology Center, University of Minnesota, Minneapolis, MN, USA, in 2009. His research interests are in detection and estimation, with emphasis on communications and radar signal processing. He is an Associate Editor of *European Association for Signal Processing* and Elsevier, and served as an Associate Editor for the IEEE TRANSACTIONS ON SIGNAL PROCESSING.

LUCA VENTURINO (Senior Member, IEEE) received the Ph.D. degree in electrical engineering from the University of Cassino and Southern Lazio, Italy, in 2006. He held short-term visiting appointments with the Mobile and Signal Processing Department, NEC Laboratories America, Princeton, NJ, USA, in 2006, 2007, and 2008, and also with the Department of Electrical Engineering, Columbia University, New York, NY, USA, in 2004, 2009, 2022, 2024, and 2025. From 2011 to 2017, he served as an external consultant for the Space and Avionics Division of Leonardo (formerly Selex ES and Selex Galileo), Nerviano, Italy. Since 2006, he has been with the Department of Electrical and Information Engineering, University of Cassino and Southern Lazio, where he is currently a Full Professor of Telecommunications. His research interests lie in the broad area of signal processing, with a focus on detection, estimation, and resource allocation for wireless communications and radar systems. He currently serves as a Senior Area Editor for the IEEE TRANSACTIONS ON SIGNAL PROCESSING. Previously, he served as a Senior Area Editor for the IEEE SIGNAL PROCESSING LETTERS and as an Associate Editor for the IEEE TRANSACTIONS ON SIGNAL PROCESSING and the IEEE SIGNAL PROCESSING LETTERS.

MARCO LOPS (Fellow, IEEE) received the Laurea and Ph.D. degrees from "Federico II" University. He was first an Assistant Professor and then an Associate Professor with the University of Naples Federico II, Italy. In 2000, he moved to the University of Cassino and Southern Lazio as a Full Professor and he returned to the University of Naples Federico II in 2018. From 2009 to 2012, he was also with ENSEEIHT, Toulouse, France, first as a Full Professor (on leave of absence from Italy) and then as a Visiting Professor. He was a Visiting Professor with the University of Minnesota in 2008 and also with Columbia University in 2009. Previously, he had also held visiting positions with the University of Connecticut, Rice University, and Princeton University. He is currently a Professor with the Department of Electrical and Information Technology, University of Naples Federico II. He has authored or co-authored more than 90 scientific papers published on refereed journals. His research interests include detection and estimation, with emphasis on communications and radar signal processing. He was a corecipient (with Ezio Biglieri) of the 2014 Best Paper Award from the *Journal of Communications and Networks*. From 2009 to 2015, he served two terms for the Sensor Array and Multichannel Signal Processing Technical Committee. He has served as an Associate Editor for *Journal of Communications and Networks*, IEEE TRANSACTIONS ON INFORMATION THEORY (Area: Detection and Estimation, two terms), IEEE SIGNAL PROCESSING LETTERS, and IEEE TRANSACTIONS ON SIGNAL PROCESSING (two terms). He also served as a Senior Area Editor for IEEE TRANSACTIONS ON SIGNAL PROCESSING. He was selected to serve as a Distinguished Lecturer for the Signal Processing Society from 2018 to 2020.